Innovative 3D printed design to conceive highly fire-retardant multi-material

Laura Geoffroy, Fabienne Samyn, Maude Jimenez, Serge Bourbigot

Version of Record: https://www.sciencedirect.com/science/article/pii/S0141391019303209
Manuscript_c009eae61e642c4907b6bf48a6325978

Innovative 3D printed design to conceive highly fire-retardant multi-material

Laura GEOFFROY [1], Fabienne SAMYN[1], Maude JIMENEZ[1], Serge BOURBIGOT[1*]

[1]Univ. Lille, CNRS, ENSCL, UMR 8207, Unité Matériaux et Transformations (UMET), F-59000 Lille, France
laura.geoffroy@univ-lille.fr (L.G.), fabienne.samyn@univ-lille.fr (F.S.), maude.jimenez@univ-lille.fr (M.J.)
[*]corresponding author: serge.bourbigot@univ-lille.fr (S.B.); Phone: +33 (0)3 20 43 48 88

Keywords: Additive manufacturing, Design, Biphasic materials, Flame retardancy

Abstract:

In this work, instead of changing the formulation of materials, modification of their design has been investigated as an alternative approach to reach optimized fire performance. Technic of choice for such purpose, fused polymer deposition has been used to create innovative flame retarded sandwich structures with two skins completely filled and a partially filled grid patterned core. In the first part, different grid patterned cores were prepared by varying the infill density (either 30 or 50 wt.-%) as well as the fire retardant used in the ethylene vinyl acetate. Three EVA formulations were used, two containing aluminum tri-hydroxide (ATH) at respectively 30 and 65 wt.-% loadings and one based on expandable graphite used at 10 wt.-%. In a second step, biphasic materials containing air, water, potassium carbonate solubilized or in powder form sodium carbonate inside the porosity of the sandwich core were evaluated in the material (composed on EVA and 30 wt.-% of ATH). A full characterization of the fire properties of these innovative 3D designs was performed. It revealed that new light design with potassium carbonate in liquid phase inside the core material reached very good flame retardant properties. It exhibited a fast flame extinguishment and strong HRR reduction. This work is a proof of concept (based on the scarce literature data) of the usefulness of fused polymer deposition technology to design new flame retarded materials, offering a way to make safer materials at low cost.

Introduction

Nowadays, the demand of polymeric materials exhibiting low reaction to fire is in constant increase in many fields such as transportation, electrical and electronics, and cable and wire. To elaborate fire retarded materials, the standard approach consists in changing the

formulation of the materials by incorporating additives, flame retardants (FRs), improving their fire behavior [1 - 4]. However, the development of new FRs remains challenging and costly. For this reason, in this work another way of thinking was considered. Instead of changing the material formulation, the influence of the design and structure of materials was studied as an alternative to reach high fire performance. Some approaches were already done with for example a skin-core structure [5 - 7]. But, the preparation of sophisticated structures using standard shaping processes such as injection or thermocompression is not straightforward and implies the use of complex molds [8]. For this reason, our approach was to take advantage of the flexibility of additive manufacturing as processing method to prepare and design flame retarded materials.

Additive manufacturing consists in building 3D objects by adding layer upon layer of materials [9]. It has three main advantages. It allows: i) to save materials, because the exact amount of needed polymer is used, ii) to save money, because no tools or molds are needed to elaborate sophisticate shapes, iii) and to be flexible to design 3D objects. Most studies using additive manufacturing are focused on the evaluation of mechanical properties [6 - 7]. Only few works have taken interest in fire performances [12 - 13]. Different additive manufacturing techniques are commercially developed and available such as stereolithography, selective laser sintering and so forth. Among all of them, fused polymer deposition technique has the best quality to cost ratio. This technique consists in feeding a polymer in the form of filaments or pellets to a heating printer extruder and depositing it on a heating plate to elaborate the 3D part. There are already some commercially available flame-retarded filaments for fused polymer deposition [14 - 20] on the market such as polyamide 6 containing phosphorus-based flame retardant from Clariant [19], as well as Kepstan PEKK and Kynar PVDR from Arkema [20]. However, the range of such products is very limited and depends on the 3D printing brand. Moreover, with fused polymer deposition technique, the development of polymer filaments is difficult because of the very good quality needed in terms of homogeneity of diameter and of the level of mechanical properties to avoid breaking. With this in mind, fused polymer deposition using directly pellets polymer seems a more appropriate technic in this work. It also allows to remove the winding step in the process, and thus save time.

In this paper, additive manufacturing was used to elaborate new designs of materials including lighter design. The possibility to print samples using different infill densities was used to prepare sandwich materials. The skins of the sandwich were made of 100% filled layers whereas the core was partially filled (Figure 1). In the first part, the fire performances

of sandwiches having grid patterned designs partially fills with 30% or 50% of flame retarded polymers were compared with a standard design (plate completely filled with 100% polymers). Then, for sandwich designs printed with a core prepared with an infill of 30%, new biphasic materials were suggested. The possibility of using the core materials as flame retardant carrier was thus investigated as illustrated in Figure 1. Water, potassium carbonate in the liquid and solid state or sodium carbonate in liquid phase were used to fill the pores of the core material. Carbonates were selected because: i) it is the major component (80%) in powder fire extinguishers by the CO_2 emission during the decarbonation [21], ii) it reveals amazing properties in fire vase concept (this vase works using potassium carbonate to quickly extinguish fire by suppressing oxygen when the vase is smashed) developed by Samsung (Seoul, South-Korea) [22]. Among all carbonates, potassium carbonate was chosen because of it high solubility coefficient in water. These new designs were elaborated using flame-retarded Ethylene Vinyl Acetate (EVA) formulations. This polymer is a model material to prove the concept and because of its softness, flexibility and polarity which makes it easy to extrude. Moreover, this widely used polyolefin was extensively studied in our laboratory [23 - 26]. These materials were characterized using optical microscopy and fire tested using Mass Loss Cone Calorimeter test (MLCC).

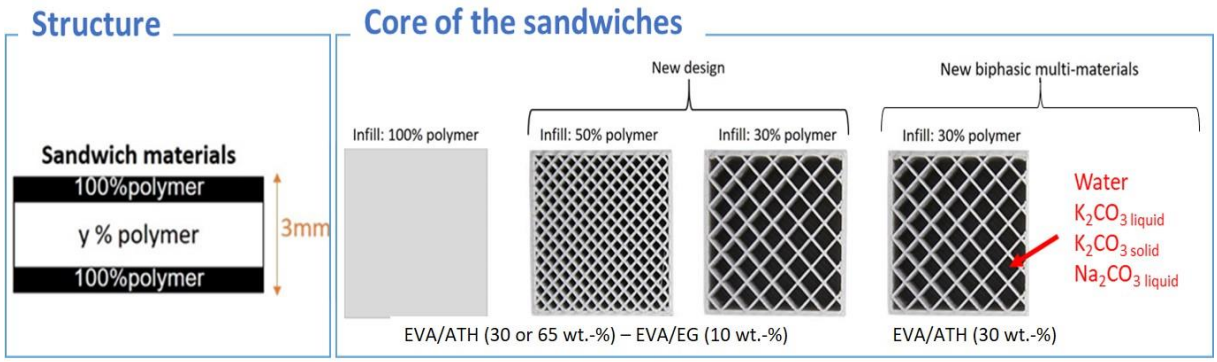

Figure 1. Concepts of FR designs printed using additive manufacturing.

Materials and methods

1. Materials

EVA (Evatane 28-05), supplied by Arkema (Colombes, France) (batch A70760804) was used as polymeric matrix. Two flame-retardants were incorporated in this matrix either Aluminum Tri-Hydroxide (ATH, Apyral 40CD, D_{50} of 1.5µm), purchased from Nabaltec (Schwandorf, Germany), and Expandable Graphite (EG, ES 350F5, 80% of particles ≥ 300 µm) purchased

from AMG graphite (Hauzenberg, Germany). These FRs were chosen because of their two different modes of action under heat flux exposure. On the one side, ATH acts in condensed phase to protect material with the formation of protective ceramic (alumina) according to an endothermic decomposition reaction (2 $Al(OH)_3 \rightarrow Al_2O_3 + 3H_2O$, ΔH=280 cal/g) coupled with a dilution effect due to water emission into gas phase [24], [25]. On the other side, EG has an intumescent behavior due to the physical expansion of the graphite worms caused by the sublimation of inserted compounds trapped between the layers [26]. An entangled network ensures a protective barrier formation.

2. Formulations

Three different materials (Table 1) were prepared using a twin-screw extruder (Thermo Scientific Rheomex OS PTW16 Haake (Vreden, Germany) with the temperature profile detailed in Figure 2. EVA pellets were introduced in the feeding zone and melted. Then, in the fourth zone, the FRs (ATH or EG) were incorporated using gravimetric feeder, and mixed with the matrix. The extrusion speed was 100 and 250 rpm for EVA/ATH and EVA/EG respectively. Finally, the strands of EVA/ATH or EVA/EG were cooled down in air and pelletized (pelletizer Thermo Scientific (Waltham, Massachusetts, United States of America)).

Table 1.Composition of materials studied.

Name of polymer materials	Weight amount of additives (%)
EVA/ATH (30 wt.-%)	30
EVA/ATH (65 wt.-%)	65
EVA/EG (10 wt.-%)	10

Figure 2. Temperature of ten heating chambers of the extruder

3. Printed samples

The pellets prepared were used to elaborate 50x50x3 mm^3 sandwich samples using a Pollen (Ivry-sur-Seine, France) 3D printer. The printer has already been fully described elsewhere

[13]. This fused polymer deposition technique consists in feeding polymers pellets from polymer container to a heater printer extruder, and depositing a fused polymer on a heating plate according to a computed pattern (Figure 3).

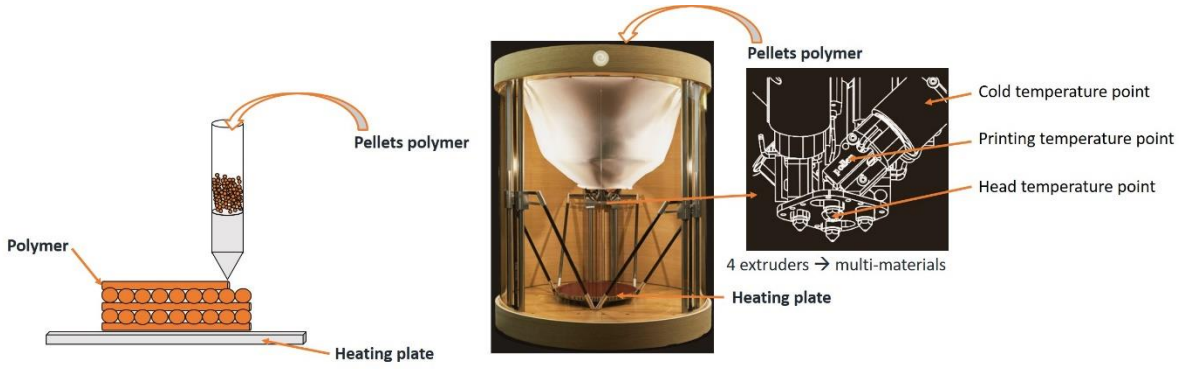

Figure 3. Illustration of the additive manufacturing technique used

The main parameters which were used to print polymer samples are defined in Table 2. Nozzle diameter was higher for EVA containing 10 wt.-% of expandable graphite because of the higher EG particle size (300 µm) than ATH particle (1.5 µm). Moreover, the bed temperature of the EVA with 65 wt.-% of ATH were higher than the other materials due to its poor adhesion onto the heating plate. The percentage of the infill (Table 2) corresponds to the amount of polymer in 3D object designed. In this work, the percentage changes from 50 to 30 according to design studied, and is equal at 100 for the standard design (considered as reference).

Table 2. Main printing parameters for each material studied

Formulation	EVA/ATH (30 wt.-%)	EVA/ATH (65 wt.-%)	EVA/EG (10 wt.-%)
Cold temperature (°C)	65	65	65
Printing temperature (°C)	130	130	130
Head temperature (°C)	225	225	200
Printing speed (mm/s)	20	20	20
Nozzle diameter (mm)	0.8	0.8	1
Bed Temperature (°C)	65	80	65
Layer height (mm)	0.3	0.3	0.3
Infill (%)	100 or 50 or 30	100 or 50 or 30	100 or 50 or 30

The Table 3 summarizes the samples prepared. Two sets of samples can be distinguished. The first nine samples concern the samples made with the three different formulations and the three infill densities (100, 50 and 30 ~~wt.~~ %). The voids in the core are let unfilled and consequently just contain air. The second set of samples is composed of samples made with the formulation EVA/ATH (30 wt.-%), an infill of 30% and a second liquid and solid phase incorporated after the printing in the voids of the core as illustrated in Figure 1. The sample without top section, and the top section were printed separately. Then a certain weight controlled amount of liquid or solid (depending on the sample studied) was put in the sample without top section. Finally, the top section was melt welded, using a heating element to make the biphasic samples. Distilled water, potassium carbonate (Aldrich, Steinheim, Germany, 98% purity) used as a powder and diluted in water (as saturated solution and as a solution with 0.05 g/ml mass concentration) and anhydrous sodium carbonate (Carlo Erba Reagenti, Barcelona, Spain) diluted in water (as a solution with 0.05 g/ml mass concentration) were used. Both carbonates (potassium and sodium) were chosen because of their high solubility coefficient in water (138 g/l and 212 g/l, respectively). Moreover, these two carbonates were studied to estimate the influence (if any) of the ion (K^+ or Na^+) in terms of fire behavior.

Table 3. Name and description of samples prepared

	Name of the sample	**Phase 1**		**Phase 2**
		Infill density (%)	**Formulation**	
1	EVA/EG (10 wt.-%)-0%air	100	EVA/ EG (10 wt.-%)	Air
2	EVA/EG (10 wt.-%)-50%air	50		
3	EVA/EG (10 wt.-%)-70%air	30		
4	EVA/ATH (65 wt.-%)-0%air	100	EVA/ ATH (65 wt.-%)	
5	EVA/ATH (65 wt.-%)-50%air	50		
6	EVA/ATH (65 wt.-%)-70%air	30		
7	EVA/ATH (30 wt.-%)-0%air	100	EVA/ ATH (30 wt.-%)	
8	EVA/ATH (30 wt.-%)-50%air	50		
9	EVA/ATH (30 wt.-%)-70%air	30		
10	EVA/ATH (30 wt.-%)-70%water	30		Water
11	EVA/ATH (30 wt.-%)-70%K_2CO_3 sat.-liquid	30		Saturated solution of K_2CO_3
12	EVA/ATH (30 wt.-%)-70%K_2CO_3 liquid	30		0.05 g/L solution of K_2CO_3
13	EVA/ATH (30 wt.-%)-70%K_2CO_3 solid	30		K_2CO_3 solid

14	EVA/ATH (30 wt.-%)-70%Na_2CO_3 liquid	30		0.05 g/L solution of Na_2CO_3

4. Fire testing: Mass Loss Cone Calorimeter (MLCC)

The reaction to fire performance of the prepared materials was evaluated using a Mass Loss Cone Calorimeter (MLCC) from Fire Testing Technology (FTT) (West Sussex, UK) according to standards ISO 13927 or ASTM E906 [27 - 28]. The equipment is similar to that used in oxygen consumption cone calorimetry (ASTME-1354-90), except that a thermopile placed in the chimney is used to obtain heat release rate (HRR) instead of employing the oxygen consumption principle. 3D printed plates samples (50x50 mm^2) placed on a ceramic backing board at a distance of 35 mm from heater were exposed in a horizontal orientation to an external heat flux 50 kW/m^2. The MLCC allows determining the following main fire properties: HRR as a function of time, peak of heat release rate (pHRR), time to ignition (TTI), and total heat release (THR). At least two MLCC experiments were performed on each material in order to ensure repeatability within the error margins of ±10% for pHRR and THR and ±15% for TTI. During the test, temperature versus time profiles were measured in the middle of the backside of the polymer plates using a K-type thermocouple (TC SA, Dardilly, France) fixed in a calsil plate. Data were recorded using a graphtec 34970A data logger (Keysight Technologies, Santa Rosa, CA, USA). Concurrently to MLCC test, gas phase analysis was done using a Fourier Transform InfraRed (FTIR) spectrometer (Antaris TM Industrial Gas System (Thermofisher, Waltham, Massachusetts, United States). A gas picking and transfer line (M&C Tech Group, Ratingen, Germany), were put on the top of chimney. The 2 m long transfer line between MLCC and FTIR is heated up at 200°C. To assure constant temperature of the transfer line, two temperature controllers are installed. Before analyzing the gases by FTIR, soot particles are filtered by two different filters (2 and 0.1µm). These filters are composed of glass fibers and ceramic respectively. The FTIR gas cell is set at 185°C and 652 Torr. The optical pathway is 2 m long and the chamber of the spectrometer is filled with dry air. FTIR spectra obtained using MLCC-FTIR are treated using OMNIC software. The spectrometer is calibrated to quantify water, carbon monoxide, and carbon dioxide. Quantification is reproducible within 10%.

5. Characterizations

5.1. Optical microscopy

Optical microscopy observations were carried out on 3D printed samples using a microscope VHX-1000 HDR (High Dynamic Range, Keyence, Osaka, Japan). Samples were analyzed in cross-section by embedding them into an epoxy resin, followed by polishing (up to 0.25 µm) using silicon carbide disks (ESCIL, Chassieu, France).

5.2. Scanning Electron Microscopy

Soot samples were collected by applying a 45x15x0.9 mm^3 mirror polished stainless-steel plate (Goodfellow, Cambridge, United Kingdom) inside the flame. The mirror polished stainless-steel plate was beforehand cleaned for 10 min in 1:1 acetone and ethanol solution (Sigma Aldrich, St. Louis, Missouri, Unites States), then put for 10 min at 65°C in a solution of water and 2% of RBST105 (Chemical products R. Borghgraef. S.A., Brussels, Belgium) which is a liquid alkaline and foaming cleaner, and finally put in water solution at room temperature for 5 min before being dried. Then, the mirror polished stainless-steel plate was applied in the flame at the pHRR [29].

Soot images and EDS analysis were acquired using a JEOL JSM 7800F LV (JEOL ltd, Tokyo, Japan) scanning electron microscopy (SEM) at 6.0 kV and 121.2 µA. To analyze samples using, a carbon coating with a Bal-Tec SCD005 sputter coater (Bal-Tec, Los Angeles, California, United States) were previously done on sample. X-ray mappings were performed using an Oxford Instruments SDD EDS detector (Abingdon, United Kingdom), coupled with Aztec software. K, Al, C, O, Ni, Fe, Cr, and Mo elements were studied (developed in 2.3). All EDS spectra, EDS mappings and images obtained were treated using Aztec software afterward.

Observations of the residues obtained after MLCC test were also carried out using the SEM. Samples were analyzed in cross-section, embedded in epoxy resin, polished and carbon coated with the same process previously detailed. EDS spectra and EDS mappings were done on some element in particular on K to investigate the mechanism.

5.3. X-Ray Diffraction (XRD)

The crystalline structure of the residues after MLCC test were determined using XRD analyses. XRD spectra were recorded in the 5° - 60° range using a Bruker AXS D8 diffractometer (Massachusetts, United States), equipped with a Cu Kα (λ = 0.154 nm)

radiation in configuration $\theta/2\theta$. All spectra obtained were analysed using DIFFRAC.EVA software (Bruker, Massachusetts, United States).

Results and discussion

1. New design of lighter flame-retardant materials with voids

1.1. Characterizations before fire testing

Top and cross-section of each sample before fire testing was observed using an optical microscope and the resulting pictures are gathered in Figure 4 and Figure 5. All samples seem quite homogeneous exhibiting the same thickness (average measured values reported in Table 4). The mass decreases according to the percentage of polymer in each plate printed. Indeed, the mass between plate polymer filled at 50% (with 50% air) and 30% (with 70% air) were -24%, -34%, -27%, -37%, -25% and -39% lower than plate completely filled with 100% of polymer for EVA/EG (10 wt.-%), EVA/ATH (30 wt.-%) and EVA/ATH (65 wt.-%) respectively. As expected, this design with 30% polymer allows to decrease the mass of material (by almost 37%, whatever the material). Lighter materials were thus elaborated. Moreover, the created grid patterns exhibit square holes of dimension around 800 µm and 1800 µm for respectively 50 and 30% infills (Table 4), whatever the materials (EVA/EG (10 wt.-%), EVA/ATH (30 wt.-%), EVA/ATH (65 wt.-%)). The holes in the grid with 50% air have length roughly half the size as the one of the grid with 70% air (Figure 4). The top and bottom thickness layers for each plate were calculated giving an averaged value equal to 604 µm, (Table 4).

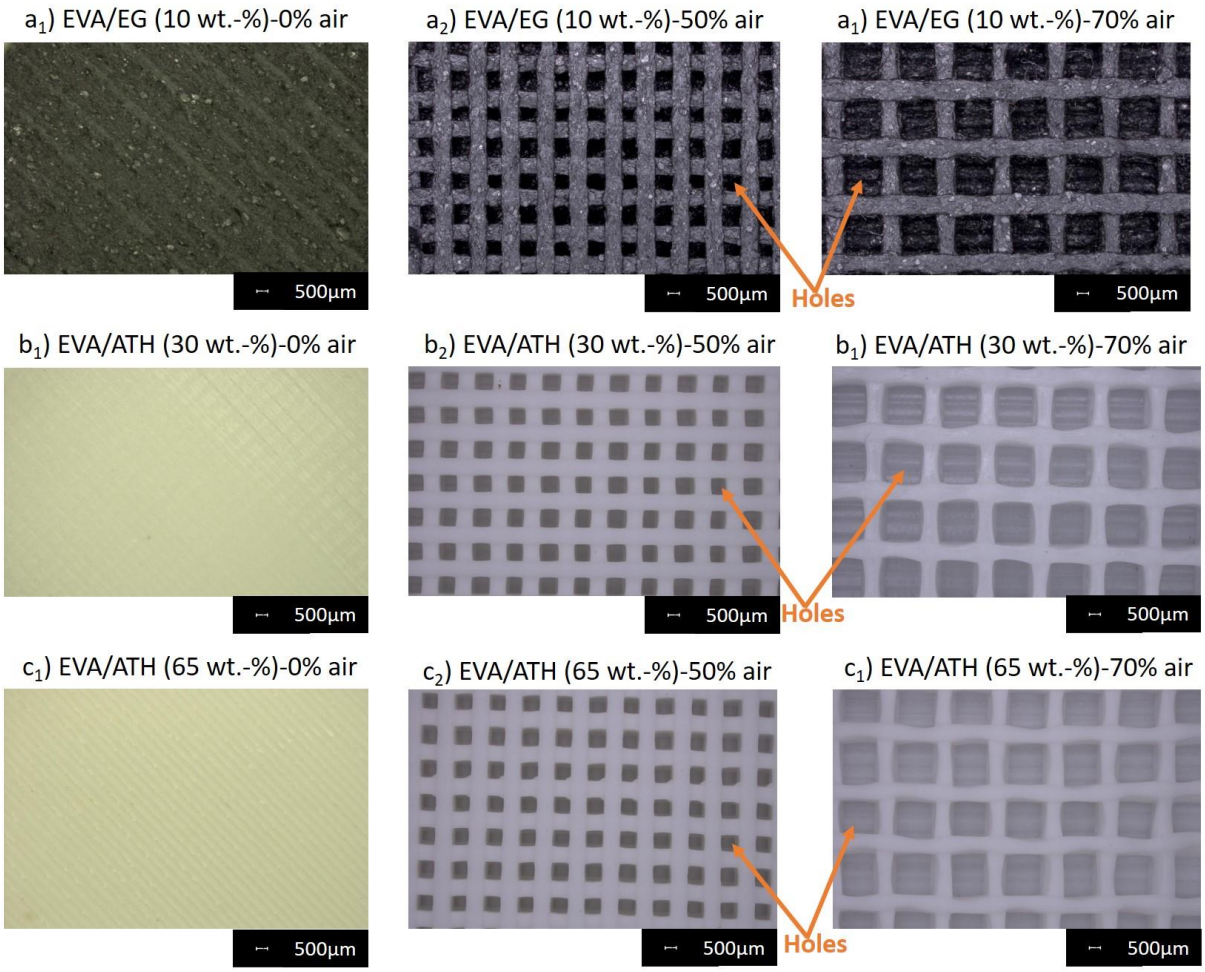

Figure 4. Top section observation using optical microscopy (x20) before MLCC test (a_1) EVA/EG (10 wt.-%)-0% air, a_2) EVA/EG (10 wt.-%)-50%, a_3) EVA/EG (10 wt.-%)-70% air, b_1) EVA/ATH (30 wt.-%)-0% air, b_2) EVA/ATH (30 wt.-%)-50% air, b_3) EVA/ATH (30 wt.-%)-70% air, c_1) EVA/ATH (65 wt.-%)-0%air, c_2) EVA/ATH (65 wt.-%)-50%air, c_3) EVA/ATH (65 wt.-%)-70%air)

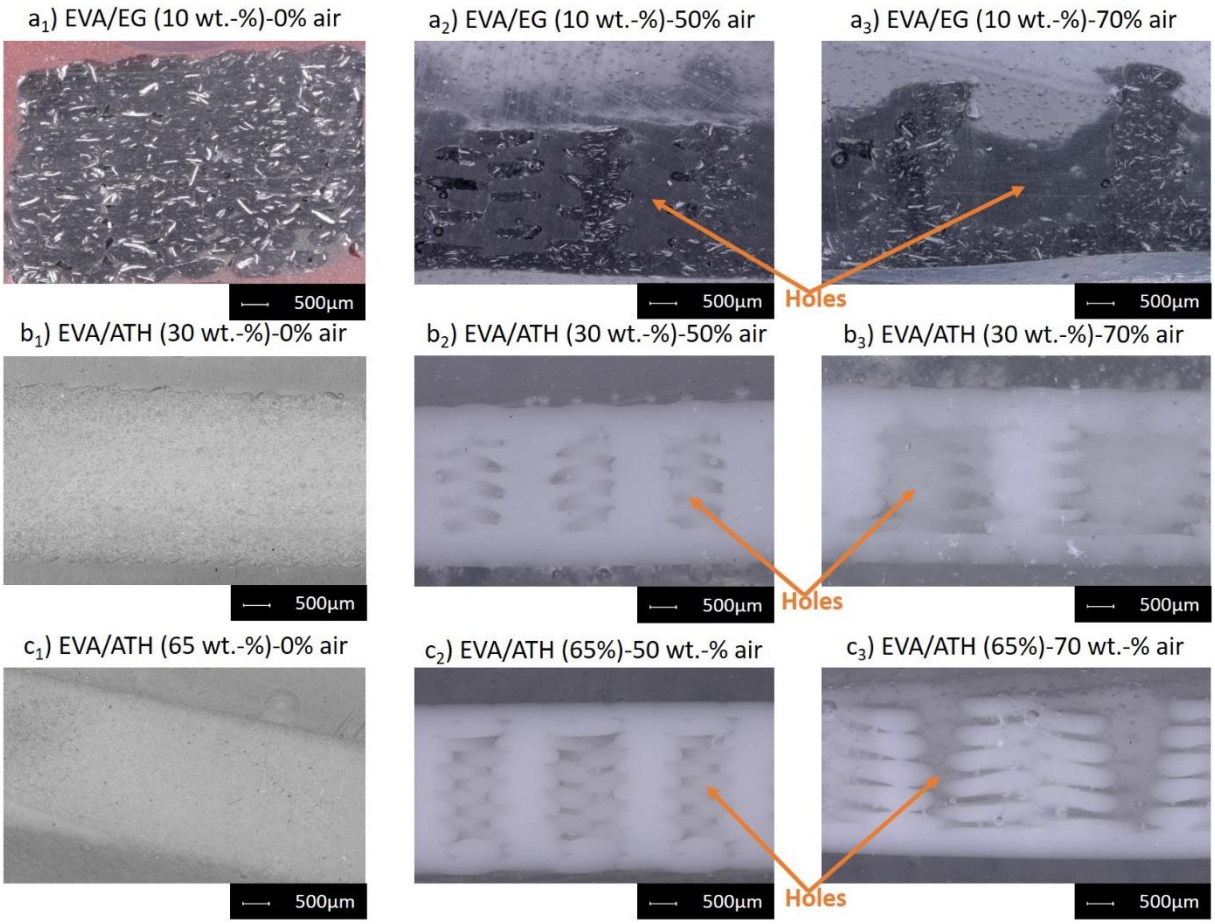

Figure 5. Cross section observations using optical microscopy (x50) before MLCC test (a_1) EVA/EG (10 wt.-%)-0% air, a_2) EVA/EG (10 wt.-%)-50%, a_3) EVA/EG (10 wt.-%)-70% air, b_1) EVA/ATH (30 wt.-%)-0% air, b_2) EVA/ATH (30 wt.-%)-50% air, b_3) EVA/ATH (30 wt.-%)-70% air, c_1) EVA/ATH (65 wt.-%)-0%air, c_2) EVA/ATH (65 wt.-%)-50%air, c_3) EVA/ATH (65 wt.-%)-70%air)

Table 4. Quantitative characterization of each sample studied

Formulation	Mass (g)	Thickness (mm)	Square hole dimension (µm)	Fused filament diameter (mm)	Bottom layer thickness (mm)
EVA/EG(10 wt.-%)-0% air	7.07 ± 0.02	3 ± 0	/	/	/
EVA/EG (10 wt.-%)-50% air	5.4 ± 0.2	3 ± 0	840	800	580
EVA/EG (10 wt.-%)-70% air	4.67 ± 0.04	3 ± 0	1800	840	605
EVA/ATH (30 wt.-%)-0% air	9.2 ± 0.3	3 ± 0	/	/	/
EVA/ATH (30 wt.-%)-50% air	6.72 ± 0.03	3 ± 0	900	820	640
EVA/ATH (30 wt.-%)-70% air	5.82 ± 0.03	3 ± 0	1770	820	590
EVA/ATH (65 wt.-%)-0% air	12.18 ± 0.04	3 ± 0	/	/	/

EVA/ATH (65 wt.-%)-50% air	9.13 ± 0.03	3 ± 0	787	820	620
EVA/ATH (65 wt.-%)-70% air	7.4 ± 0.2	3 ± 0	1830	840	590

1.2. Fire protection performances

Reaction to fire of plates with 70% air (30% polymer) and 50% air (50% polymer) were compared to those of completely filled (100% polymers, standard design). Figure 7 and Table 5 show HRR as a function of time curves and the averaged values of pHRR, THR and TTI for the different systems (EVA/EG (10 wt.-%), EVA/ATH (30 wt.-%), and EVA/ATH (65 wt.-%)).

It is observed that systems with 65 wt.-% ATH and 10 wt.-% EG were very efficient compared to system with 30 wt.-% ATH whatever the design studied. pHRR of standard design plate (100% polymers) of EVA/ATH (30 wt.-%) were 88% and 150% higher than that of systems with the standard design containing 10 wt.-% of expandable graphite and 65 wt.-% ATH, respectively (an increase of 65% and 71% was also obtained for the THR of both materials (with EG and 65 wt.-% ATH respectively)). It is consistent with results reported in a previous study [139]. It is noteworthy that sandwich designs containing voids exhibit better performance than the 100% filled reference plates whatever the material. It makes sense because in these cases there is less polymer and consequently less fuel.

For the EVA/EG (10 wt.-%) material (Figure 7 a)), the results are identical for the two infills (70% air compared to 50% air) in terms of THR, pHRR and TTI (-6%, -1% and 3%, respectively). Compared to the reference plate without voids, pHRR and THR of plate with 70% air are decreased (by -20% and -65% respectively) what is not the case of the TTI that is unchanged. The decrease of HRR when voids are incorporated inside materials can be explained by the compacity changing of the entangled network structure caused by the voids (due to the design modification), and also by the reduction of 'fuel' load in the system. Indeed, air inside materials and thus higher porosity creates higher gap to be filled by the graphite worms and hence, it modifies the compacity of the graphite worms network (Figure 6) [13]. This structure modification can have an influence on fire protection properties as it is the case on intumescent system [30]. It is also noteworthy that hollow structure has much lower thermal conductivity comparing to non-hollow structure. Therefore, as long as the voids stand during burning, it is reasonable to assume that holes slow down the heat transfer within

the material and thus decrease the THR. Moreover, the reduction of 'fuel' load modifies the combustion and improves the fire performance.

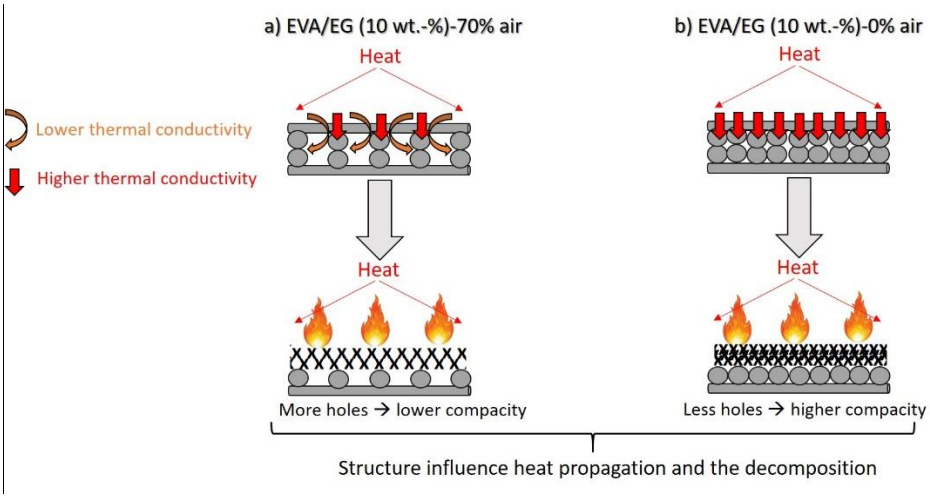

Figure 6. Compacity difference and influence in heat propagation for system (a) EVA/EG (10 wt.-%)-70% air, b) EVA/EG (10 wt.-%)-0% air)

In the case of EVA/ATH (30 wt.-%) (Figure 7 b)), the THR, the pHRR and TTI differences between the plate with 30% polymer and the plate completely fill are respectively of -37%, -12% and -37%. Regarding the comparison between EVA/ATH (30 wt.-%)-50% air and EVA/ATH (30 wt.-%)-0% air, the difference in terms of THR, pHRR and TTI is -19%, -10% and -28% respectively. Thus, for this material, the design modification does not allow to reach a significant improvement in terms of reaction to fire. In this case it seems that the FR used at this loading is not high enough to be efficient. Consequently, the sample under heat exposure, melts and burns and hence, all the voids collapse: the design is then no longer a governing parameter.

For the materials containing 65 wt.-% ATH (Figure 7 c)), there is a huge impact of the infill density on the fire performances. THR difference between 70% air plate and 50% air plate is -8 MJ/m^2, (corresponding to -29% difference) but the pHRR and TTI remain similar. Furthermore, the comparison between plain plate (standard design) and plate with 70% air revealed unexpected results. During the fire testing of EVA/ATH (65 wt.-%)-70% air, ignition started quickly when the sample was exposed to heat flux. EVA melts, burns and concurrently ATH dehydrates and makes an alumina-type ceramic (with a water dilution effect in the gas phase). The combination of water evolution, ceramization and lower 'fuel' load makes the material poorly flammable and flame extinguishment is rapidly observed. Moreover, the new design with voids inside (EVA/ATH (65 wt.-%)-70% air and EVA/ATH (65 wt.-%)-50% air) reduces the thermal conductivity of the system compared to standard design (EVA/ATH (65%

wt.-%)-0% air). Indeed, while the voids (created by the design) is maintained during the combustion, they can slow down the heat propagation, and thus improve the fire protection. So, the pHRR of EVA/ATH (65 wt.-%)-70% air was decreased by 23% compared to EVA/ATH (65 wt.-%)-0% air. Moreover, a significant reduction of THR (by 57%) was also measured but TTI is decreased by 49% for the design with 70% air inside materials (probably due to higher concentration of oxidizer (O_2 of the air filling the voids)). TTI reduction for 3D printed plates were expected as it was previously highlighted in paper [14]. Overall, the design has a strong influence and can improve the fire retardancy of materials.

A THR comparison of all systems studied was also done (Table) with the normalization of THR by sample weight to rule out the influence of mass. The same trend is found and thus a reduction of THR is obtained for EVA/EG (10%) and EVA/ATH (65%) with 50% air and 70% air. Indeed, THR of EVA/EG (10%)-70% air and EVA/EG (10%)-50% air is reduced by 46% and 51% respectively, compared to EVA/EG (10%)-0% air. Concerning EVA/ATH (65%)-70% air and EVA/ATH (65%)-50% air, THR decrease by 29 and 19% respectively, compared to EVA/ATH (65%)-0% air. No improvement of THR is measured for EVA/ATH (30%) (whatever the percentage of infill).

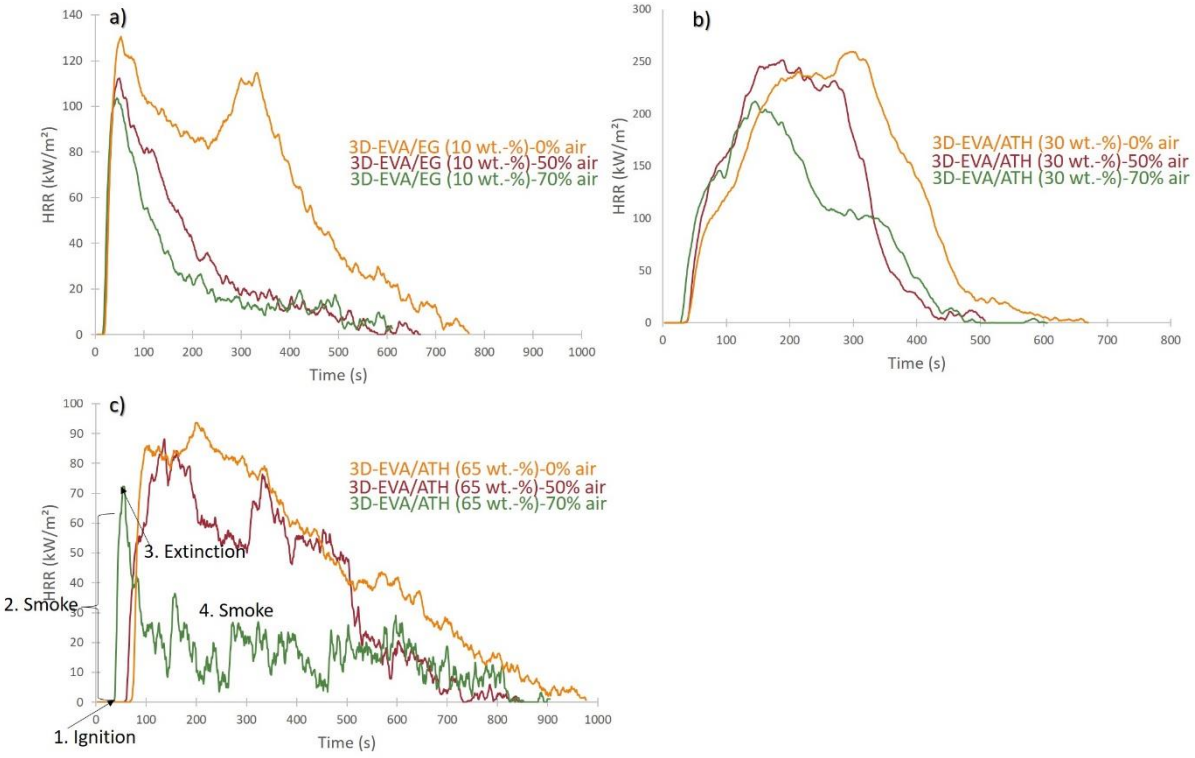

Figure 7. Influence of the design and the amount of voids on fire behavior (a) EVA/EG (10 wt.-%), b) EVA/ATH (30 wt.-%), c) EVA/ATH (65 wt.-%))

Table 5. Fire performance values of each design studied for the different formulations

Polymer matrix	TTI (s)	THR (MJ/m²)	THR/mass (MJ/m².g)	pHRR (kW/m²)
EVA/EG(10 wt.-%)-0% air	17	48	6.8	137
EVA/EG (10 wt.-%)-50% air	14.5 (-15%)	18 (-63%)	3.3 (-51%)	110 (-20%)
EVA/EG (10 wt.-%)-70% air	15 (-12%)	17 (-65%)	3.6 (-46%)	109 (-20%)
EVA/ATH (30 wt.-%)-0% air	41	79	8.6	257
EVA/ATH (30 wt.-%)-50% air	36 (-12%)	61 (-23%)	9.1 (6%)	249 (-3%)
EVA/ATH (30 wt.-%)-70% air	26 (-37%)	49.4 (-37%)	8.5 (-1%)	225 (-12%)
EVA/ATH (65 wt.-%)-0% air	73	46	3.8	103
EVA/ATH (65 wt.-%)-50% air	43.5 (-40%)	28 (-39%)	3.1 (-19%)	95 (-8%)
EVA/ATH (65 wt.-%)-70% air	37.5 (-49%)	20 (-57%)	2.7 (-29%)	79 (-23%)

Pictures of the residues after fire testing are presented on Figure 8. No additional information was obtained from the observation of the residues of EVA/EG (10 wt.-%) and EVA/ATH (30 wt.-%). For these formulations, residues are the same whatever the infill density. But, in the case of EVA/ATH (65 wt.-%), it can be distinguished that the structure is kept during the MLCC test. Indeed, the structure of the residue exhibit holes (induced by the design) below the top layer (Figure 8 c_3)). Table 6 gathers the mass loss of each sample studied. It is noteworthy that whatever the materials studied, the mass loss is almost the same for each design studied (0% air, 50% air, 70% air).

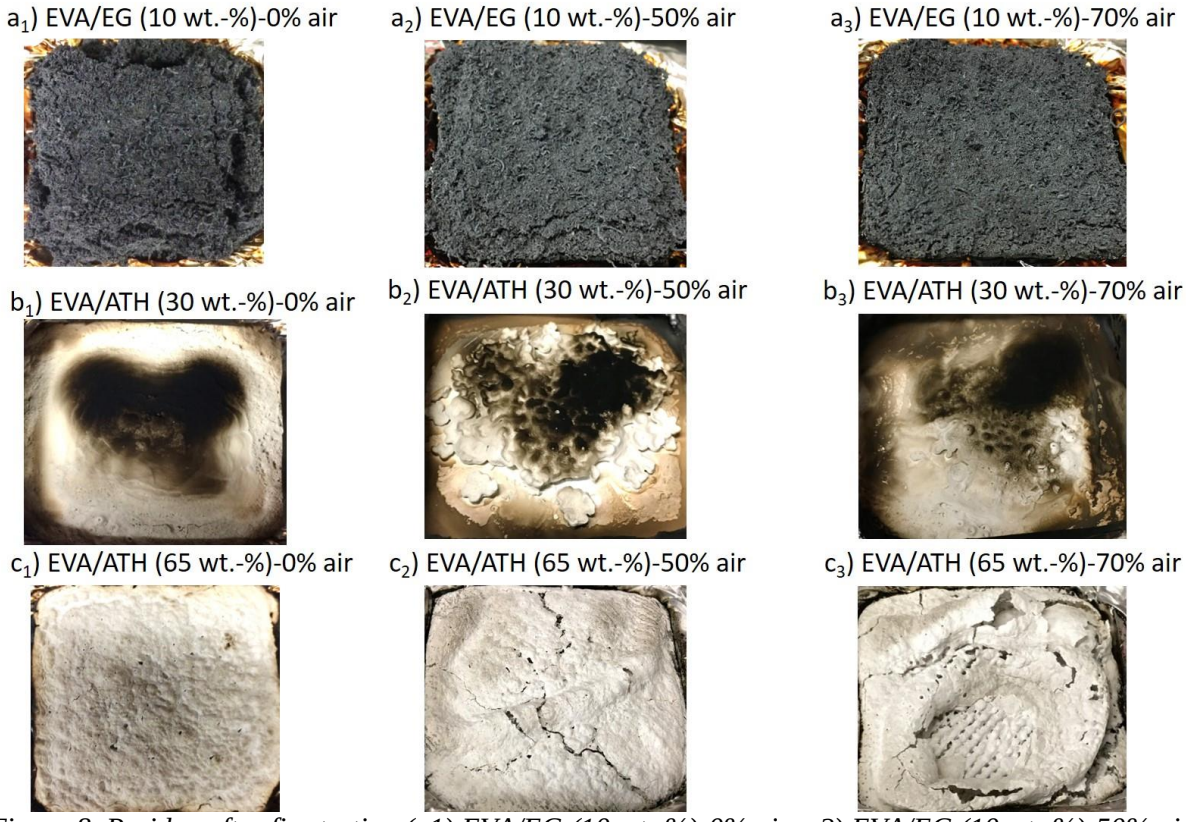

Figure 8. Residue after fire testing (a1) EVA/EG (10 wt.-%)-0% air, a2) EVA/EG (10 wt.-%)-50% air, a3) EVA/EG (10 wt.-%)-70% air, b1) EVA/ATH (30 wt.-%)-0% air, b2) EVA/ATH (30 wt.-%)-50% air, b3) EVA/ATH (30 wt.-%)-70% air, c1) EVA/ATH (65 wt.-%)-0% air, c2) EVA/ATH (65 wt.-%)-50% air, c3) EVA/ATH (65 wt.-%)-70% air)

Table 6. Mass loss comparison between different design studied for each material (EVA/EG (10 wt.-%), EVA/ATH (30 wt.-%), EVA/ATH (65 wt.-%))

Polymer matrix	Mass (g)	Residual mass (g)	Mass Loss (%)
EVA/EG(10 wt.-%)-0% air	7.07 ± 0.02	2.675 ± 0.003	62
EVA/EG (10 wt.-%)-50% air	5.4 ± 0.2	2.61 ± 0.05	52
EVA/EG (10 wt.-%)-70% air	4.67 ± 0.03	1.7 ± 0.1	57

EVA/ATH (30 wt.-%)-0% air	9.2 ± 0.3	1.7 ± 0.1	81
EVA/ATH (30 wt.-%)-50% air	6.72 ± 0.03	1.338 ± 0.006	80
EVA/ATH (30 wt.-%)-70% air	5.82 ± 0.03	1.2 ± 0.1	79
EVA/ATH (65 wt.-%)-0% air	12.18 ± 0.04	6.6 ± 0.3	46
EVA/ATH (65 wt.-%)-50% air	9.13 ± 0.03	4.1 ± 0.2	55
EVA/ATH (65 wt.-%)-70% air	7.7 ± 0.1	3.7 ± 0.3	52

In the second part of this paper, the work focuses on the design with 70% air and 30% polymers and considering only EVA/ATH (30 wt.-%). Indeed, EVA/ATH (65 wt.-%)-70% air exhibits already extremely high fire retardancy, and it does not need any further enhancement. Regarding EVA/EG (10 wt.-%), it makes an expanded intumescent coating (and powdered residue) which is not compatible with the strategy of flame retardancy we wanted to examine (see the next section).

2. Flame retardant biphasic materials elaboration

2.1. Characterization before fire testing

Based on the same design described in the previous section, EVA/ATH (30 wt.-%)-70% air plates were elaborated (Figure 1). These plates were filled with water, potassium carbonate in liquid and solid phase, and sodium carbonate in liquid phase, and hereafter called: EVA/ATH (30 wt.-%)-70% water, EVA/ATH (30 wt.-%)-70% $K_2CO_{3\ sat.\text{-}liquid}$, EVA/ATH (30 wt.-%)-70% $K_2CO_{3\ liquid}$, EVA/ATH (30 wt.-%)-70% $K_2CO_{3\ solid}$, EVA/ATH (30 wt.-%)-70% $Na_2CO_{3\ liquid}$, respectively. Potassium and sodium carbonates were chosen due to their high solubility coefficient in water. These plates were characterized in terms of mass, thickness and liquid (or solid) phase amount, and all data are gathered in Table 7. Based on Table 7, the amount of liquid (solid) is similar regardless of the system studied (1.5 ml, 1.2 g, 1.7 ml, 1.7 ml for water, $K_2CO_{3\ solid}$, $K_2CO_{3\ liquid}$ and $Na_2CO_{3\ liquid}$, respectively), except for the system with a saturate concentration of $K_2CO_{3\ sat.\text{-}liquid}$ due to the higher density of the solution.

Table 7. Quantitative values of each biphasic material studied

Polymer matrix	Mass (g)	Thickness (mm)	Liquid / solid amount (ml or g)
EVA/ATH (30 wt.-%)-0% air	9.2 ± 0.3	3 ± 0	/

EVA/ATH (30 wt.-%)-70% air	5.82 ± 0.03	3 ± 0	/
EVA/ATH (30 wt.-%)-70% water	8.3 ± 0.2	3 ± 0.2	1.51 ± 0.1
EVA/ATH (30 wt.-%)-70% K_2CO_3 solid	7.33 ± 0.01	3 ± 0.2	1.204 ± 0.008
EVA/ATH (30 wt.-%)-70% K_2CO_3 sat.-liquid	9.4 ± 0.2	3 ± 0.2	2.6 ± 0.2
EVA/ATH (30 wt.-%)-70% K_2CO_3 liquid	8.2 ± 0.4	3 ± 0.2	1.7 ± 0.5
EVA/ATH (30 wt.-%)-70% Na_2CO_3 liquid	8.2 ± 0.4	3 ± 0.2	1.7 ± 0.5

2.2. MLCC fire testing

Figure 9 and Table 8 show the fire behavior of each filled sample (HRR vs time) and the associated fire parameters (TTI, THR and pHRR). The graph clearly evidences a difference of behavior between the samples.

On one hand, when voids were filled with water or powdered K_2CO_3, no significant improvement were recorded compared to EVA/ATH (30 wt.-%)-70% air. All TTI were either similar or lower than unfilled core sample (-19% and 2% respectively), and the THR as well as the pHRR are of the same order of magnitude or even slightly higher (32% and 7% for the THR respectively, and 13% and 4% for the pHRR respectively). Therefore, no benefits are achieved when air is substituted by water or powdered K_2CO_3.

On the other hand, when solutions with same mass concentration of K_2CO_3 or Na_2CO_3 are used, a dramatic decrease of the pHRR (by -80% and -72% respectively) and THR (by -75% and -71% respectively) as well as an increase of the TTI (31% and 42%, respectively) are achieved. These enhanced performances can be explained by the fast flame extinction observed during the experiments (visual observation). This extinction is obtained using saturated (112 g/L) and diluted (0.05 g/L) solution of K_2CO_3. Therefore, it is reasonable to assume that the concentration difference between these two solutions does not influence significantly the fire performance of the material and neither does the cation of the carbonate salts used.

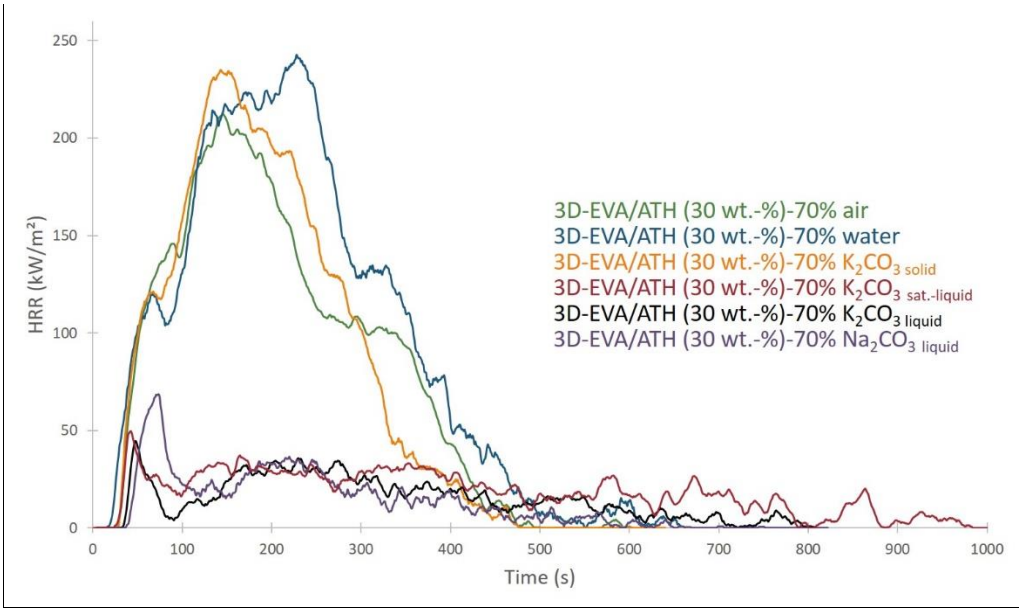

Figure 9. Comparison of the fire behavior of biphasic multi-materials

Table 8. Fire protection performances values of each system studied

Polymer matrix	TTI (s)	THR (MJ/m²)	pHRR (kW/m²)
EVA/ATH (30 wt.-%)-70% air	26	49.4	225
EVA/ATH (30 wt.-%)-70% water	21 (-19%)	65 (32%)	255 (13%)
EVA/ATH (30 wt.-%)-70% K_2CO_3 solid	26.5 (2%)	53 (7%)	235 (4%)
EVA/ATH (30 wt.-%)-70% K_2CO_3 sat.-liquid	34 (31%)	17.5 (-65%)	52 (-77%)
EVA/ATH (30 wt.-%)-70% K_2CO_3 liquid	34 (31%)	12.4 (-75%)	46 (-80%)
EVA/ATH (30 wt.-%)-70% Na_2CO_3 liquid	37 (42%)	14 (-71%)	62 (-72%)

During the MLCC test, a thermocouple was embedded on the backside of the material and temperature was recorded as a function of time for all systems (Figure 10, note Na_2CO_3 was not considered because of the negligible influence of the cation). Temperature progressively increases from the system with K_2CO_3 sat.-liquid, K_2CO_3 solid, water to the system with air (Figure 10). In the case of EVA/ATH (30 wt.-%)-70% air, and EVA/ATH (30 wt.-%)-70% water, four rates of change of temperature are observed until the plateau at 500°C for all samples. For the system with K_2CO_3 sat.-liquid and K_2CO_3 solid, five main changes in the slope of the temperature/time curve can be distinguished. (Table 9). From 0 s to 70 s, the heating rate of the system with K_2CO_3 in liquid and solid phase is twice as low as for EVA/ATH (30 wt.-%)-

70% air. For EVA/ATH (30 wt.-%)-70% water, the heating rate from 0 s to 70 s is 1.7-time lower than that for system with air. From 70 s to 120 s, the heating rate of EVA/ATH (30 wt.-%)-70% air is 10, 2.7 and 1.9 times higher than those of the systems with $K_2CO_{3\ sat.liquid}$, $K_2CO_{3\ solid}$ and water, respectively.

For EVA/ATH (30 wt.-%)-70% air, the temperature rise can be explained by the fact that, when the sample ignites, EVA melts and burns, thus, all voids collapse, and thus temperature grows rapidly. Comparatively, the system with water ignites and burns and at 100°C water boils (vaporization of water) but no plateau is observed (Figure 10). For the system with K_2CO_3 in solid phase, when the sample ignites, EVA melts and burns, but K_2CO_3 powdered does not decarbonize because the external heat flux is too low to make the decarbonation of K_2CO_3 (891°C). So, the powdered K_2CO_3 keeps the design at the beginning of the test and hence, it limits the temperature rise in the system. For EVA/ATH (30 wt.-%)-70% $K_2CO_{3\ sat.-liquid}$, a plateau is clearly observed at 100 s – 120 s. Temperature rise is delayed and highlights the benefit of this systems compared to the others. After 300 s, systems with water and K_2CO_3 in liquid and solid phase reach the same temperature (400°C). All the systems reach a steady-state temperature of 500°C after 450 s.

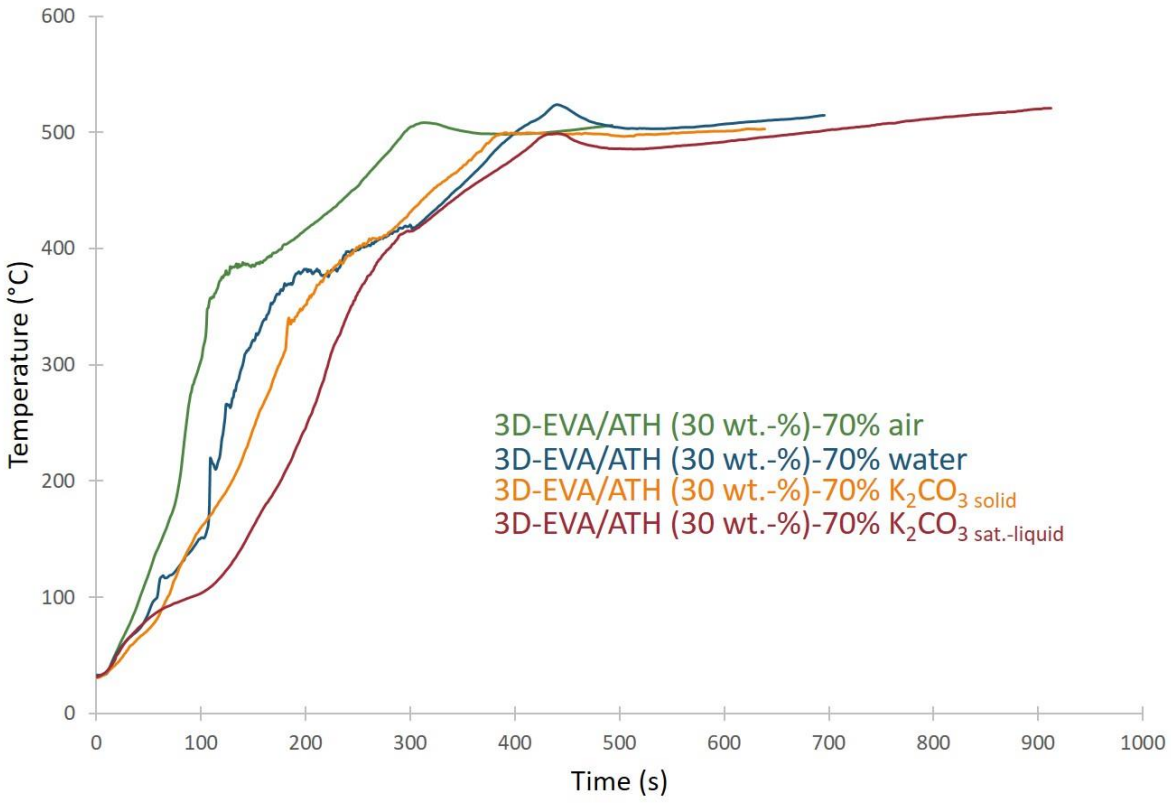

Figure 10. Evolution of temperature vs time for each biphasic material studied

Table 9. Rate of change of temperature for each sample studied.

Polymer matrix	Rates of change of Temperature (°C/s)				
	0 s – 70 s	70 s – 120 s	120 s – 200 s	200 s -300 s	300 s - 400 s
EVA/ATH (30 wt.-%)-70% air	2.14	4.51	0.73	0.73	
EVA/ATH (30 wt.-%)-70% water	1.29	2.41	2.41	0.53	0.53
EVA/ATH (30 wt.-%)-70% $K_2CO_{3\ solid}$	0.94	1.68	2.27	0.69	0.72
EVA/ATH (30 wt.-%)-70% $K_2CO_{3\ sat.-liquid}$	1.07	0.44	1.86	1.86	0.61

Pictures of the residues after fire testing and the percentage of mass loss are gathered on Figure 11 and Table 10. According to Table 10, the mass loss of sample with water is almost the same as EVA/ATH (30 wt.-%)-70% air. A slight lower mass loss is obtained for sample with K_2CO_3 in solid and liquid phase (60% and 69% respectively) compared to 79% for EVA/ATH (30 wt.-%)-70% air. A small difference is observed for the systems containing K_2CO_3 solid and K_2CO_3 liquid despite the strong THR reduction obtained for EVA/ATH (30 wt.-%)-70% $K_2CO_{3\ sat.-liquid}$. This comparison emphasizes that EVA/ATH (30 wt.-%)-70% $K_2CO_{3\ sat.-liquid}$ limits the contribution of fire growth but it does not allow protecting the material against combustion (no limitation of mass loss compared to the other systems). Moreover, a ceramic residue is obtained for each sample (Figure 11), but a different aspect is observed in the case of system with K_2CO_3 in liquid or solid phase. For EVA/ATH (65 wt.-%)-70% $K_2CO_{3\ solid}$, it is noteworthy that the residue is more gray than the others. For EVA/ATH (30 wt.-%)-70% $K_2CO_{3\ sat.-liquid}$, some white color areas are observed in comparison with the other residues. Further investigations are needed to explain these differences and they are done in the next part.

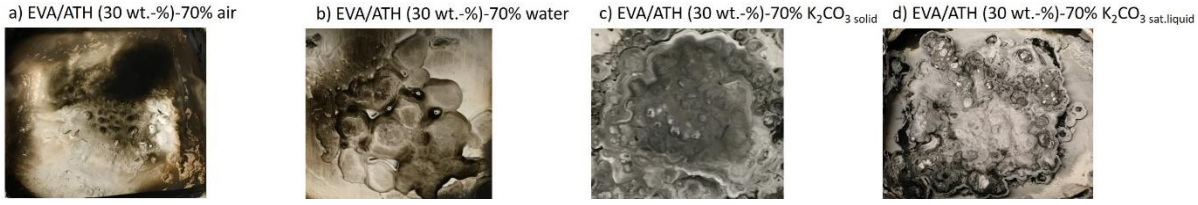

Figure 11. Residues after fire testing (a) EVA/ATH (30 wt.-%)-70% air, b) EVA/ATH (30 wt.-%)-70% water, c) EVA/ATH (30 wt.-%)-70% $K_2CO_{3\ solid}$, d) EVA/ATH (30 wt.-%)-70% $K_2CO_{3\ sat.-liquid}$)

Table 10. Mass loss comparison between each sample studied

Polymer matrix	Mass (g)	Residual mass (g)	Mass loss (%)
EVA/ATH (30 wt.-%)-70% air	5.82 ± 0.03	1.2 ± 0.1	79
EVA/ATH (30 wt.-%)-70% water	8.3 ± 0.2	1.5 ± 0.08	82
EVA/ATH (30 wt.-%)-70% $K_2CO_{3\ solid}$	7.33 ± 0.01	2.6 ± 0.3	60
EVA/ATH (30 wt.-%)-70% $K_2CO_{3\ sat.-liquid}$	9.3 ± 0.2	2.9 ±0.2	69

2.3. Mechanism investigation

2.3.1. Gas phase analysis

The system containing diluted K_2CO_3 in water exhibits an unexpected behavior and the mechanism of action were investigated in the gas and condensed phases. The flame aspect was firstly visually observed as illustrated in Figure 12. It is clearly seen that the flame obtained for EVA/ATH (30 wt.-%)-70% $K_2CO_{3\ sat.-liquid}$ is purple compared to the flame with EVA/ATH (30 wt.-%) and EVA/ATH (30 wt.-%)-70% $K_2CO_{3\ solid}$ which is more yellowish in both cases. This flame color difference might be explained by the presence of potassium ion in the flame. Indeed, the flame color is related to the de-excitation of thermally excited electrons in the form of radiation [31]. The electrons of the atoms are placed on levels with a specific energy. During heat excitation, electrons move from stable to unstable levels (higher in energy). By de-exciting themselves, they return to their original level and emit a photon (light) of a very precise wavelength (color). The wavelength of this radiation thus depends on the electronic structure of the chemical element. Therefore, certain cations such as Cu^{2+}, Sr^{2+}, Na^{+}, or K^{+} have a specific line spectrum and therefore a specific flame color associated (which is green, red, yellow/orange, and purple respectively). This observation (Figure 12) suggests therefore the presence potassium in flame, and thus in the gas phase.

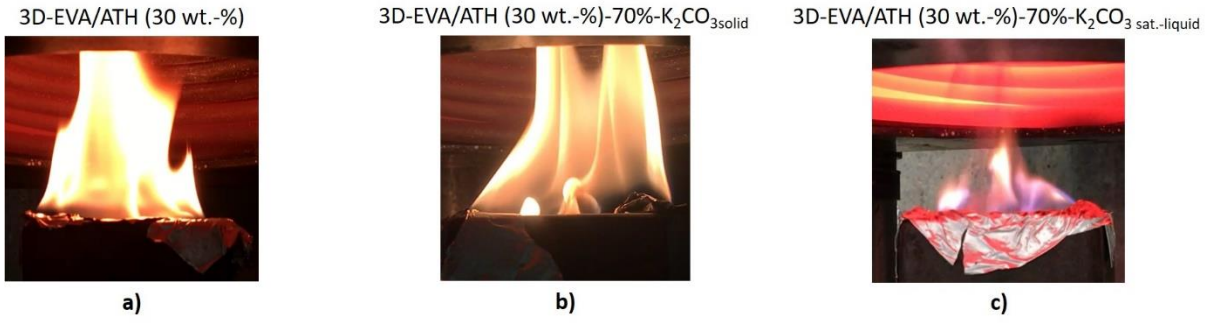

Figure 12. Flame aspect after almost 40s MLCC test (a) 3D-EVA/ATH (30 wt.-%), b) EVA/ATH (30 wt.-%)-70%-$K_2CO_{3\ solid}$, c) EVA/ATH (30 wt.-%)-70% $K_2CO_{3\ sat.-liquid}$)

To make sure of the presence of potassium in gas phase, soot was collected at pHRR during the MLCC tests (because of the higher soot particles emission [29]) using mirror polished stainless-steel plate. Then, soot particles were observed by SEM and qualitatively characterized using EDS analysis. Note that quantitative element analysis could not be done due to the difference of soot thickness deposition onto the mirror polished stainless steel. Indeed, electron beam does not impact the soot at the same electronic interaction distance. Therefore, the generation of X-rays is affected by the local specimen due to the electron penetration differences [32], and thus the quantitative comparison cannot be done in our case. Figure 13 shows the characterization of soot from EVA/ATH (30 wt.-%)-70% air, EVA/ATH (30 wt.-%)-70% water, EVA/ATH (30 wt.-%)-70% $K_2CO_{3\ sat.-liquid}$ and EVA/ATH (30 wt.-%)-70% $K_2CO_{3\ solid}$. On these graphs, Cr, Fe, Ni, Mo, Al, C and O elements are identified and come from mirror polished stainless steel, as illustrated in Figure 13 e). The presence of C and O is also due to the soot composition. In the case of the system with K_2CO_3 in liquid phase, the characteristic peak of potassium (between 3.2 and 3.4 keV) is clearly detected in the soot particles contrary to all the other systems including that with K_2CO_3 in solid phase (Figure 13).

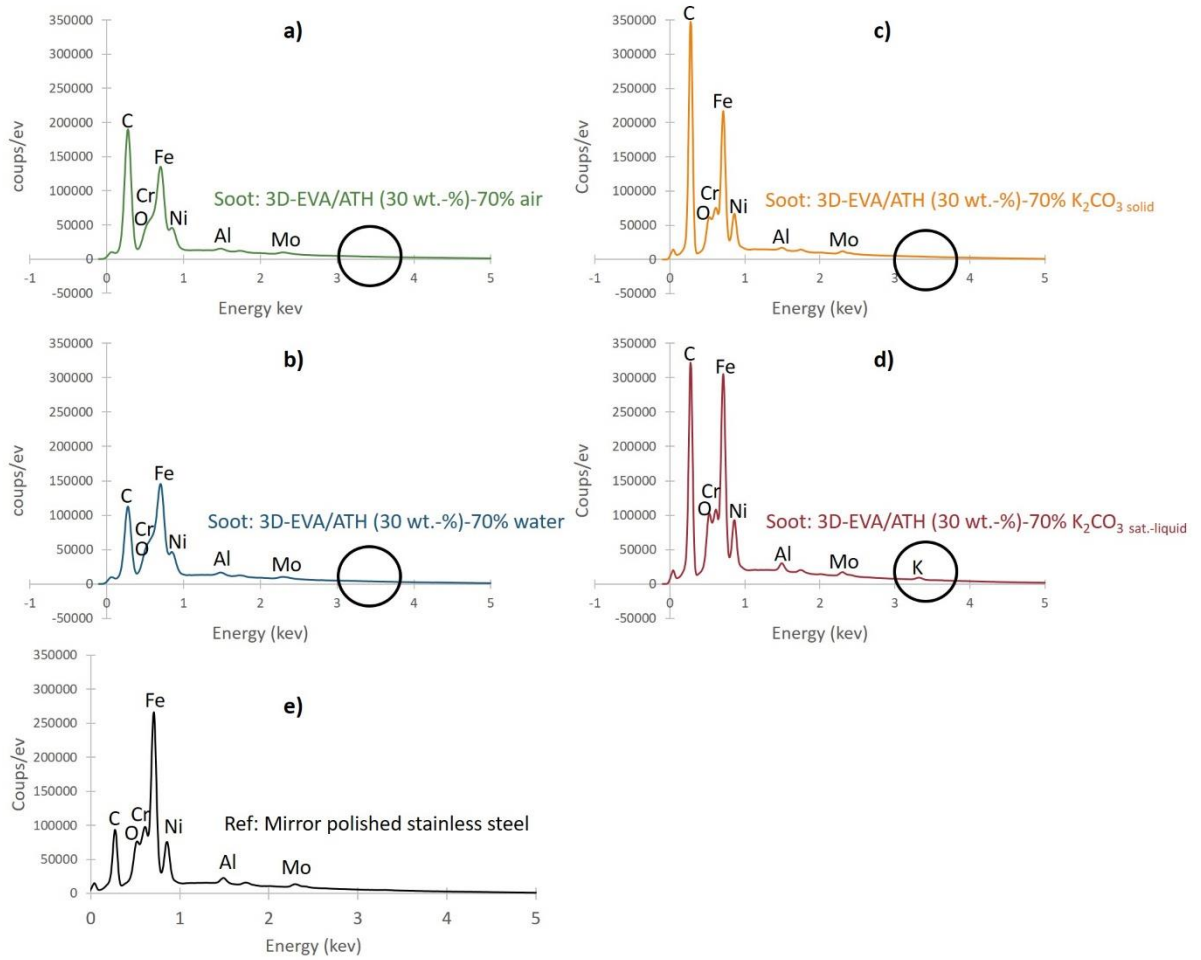

Figure 13. Soot particles EDS spectra of: a) EVA/ATH (30 wt.-%)-70% air, b) EVA/ATH (30 wt.-%)-70% water, c) EVA/ATH (30 wt.-%)-70% $K_2CO_{3\ solid}$, d) EVA/ATH (30 wt.-%)-70% $K_2CO_{3\ sat.-liquid}$, e) Mirror polished stainless steel

Finally, to better understand the gas phase combustion mechanism, the amount CO, CO_2 and H_2O evolved as a function of time during the cone experiments were plotted for each sample studied (Figure 14). Whatever the gas, EVA/ATH (30 wt.-%)-70% air, EVA/ATH (30 wt.-%)-70% water and EVA/ATH (30 wt.-%)-70% $K_2CO_{3\ solid}$ exhibit the same behavior and the curves are almost superimposed. EVA/ATH (30 wt.-%)70% $K_2CO_{3\ sat.-liquid}$ releases less quantity of water (peaks at 2.5 10^7 ppm compared to 3.5 10^7 ppm for other system studied). But, the water emission of EVA/ATH (30 wt.-%)70% $K_2CO_{3\ sat.-liquid}$ is spread over time (from 2.5 10^7 to 1.5 10^7 ppm, until 500 s MLCC test) compared to the other systems where a peak is reached at 200 s and decreasing rapidly after. The comparison of CO_2 and CO release points out that EVA/ATH (30 wt.-%)-70% $K_2CO_{3\ sat.-liquid}$ has a different behavior compared to the other samples. The system with $K_2CO_{3\ sat.-liquid}$ releases less CO_2 and more CO gases compared to the other systems (Figure 14 a) and b)). Indeed, as regards CO_2 release for EVA/ATH (30 wt.-%)-70% $K_2CO_{3\ sat.-liquid}$, a peak at 10^7 ppm is reached after 30 s MLCC test

and dramatically reduced afterward, unlike other systems where a 3.5 times higher peak is reached and maintained to $2.5.10^7$ ppm until 400 s. Regarding CO release (Figure 14 a)), a higher CO emission is observed for EVA/ATH (30 wt.-%)-70% K_2CO_3 sat.-liquid (peak at 90 ppm), compared to the other systems. Based on the comparison between CO and CO_2 emission release, a more incomplete combustion occurred for EVA/ATH (30 wt.-%)-70% K_2CO_3 sat.-liquid, compared to the other systems. Indeed, Figure 14 d) shows the CO/CO_2 ratio evolution during the MLCC test. For EVA/ATH (30 wt.-%)-70% K_2CO_3 sat.-liquid, the CO/CO_2 ratio immediately increases when sample ignites, and remains high during the MLCC test. In comparison, this ratio is low until 300 s for EVA/ATH (30 wt.-%)-70% air and until 400 s for EVA/ATH (30 wt.-%)-70% water and EVA/ATH (30 wt.-%)-70% K_2CO_3 solid, and then increases and reaches the same value as EVA/ATH (30 wt.-%)-70% K_2CO_3 sat.-liquid. These differences highlight that reactions in gas phase at the beginning of test, release less energy because of the higher CO/CO_2 ratio, and thus a more incomplete combustion occurs for the system with K_2CO_3 liquid, compared to the other samples.

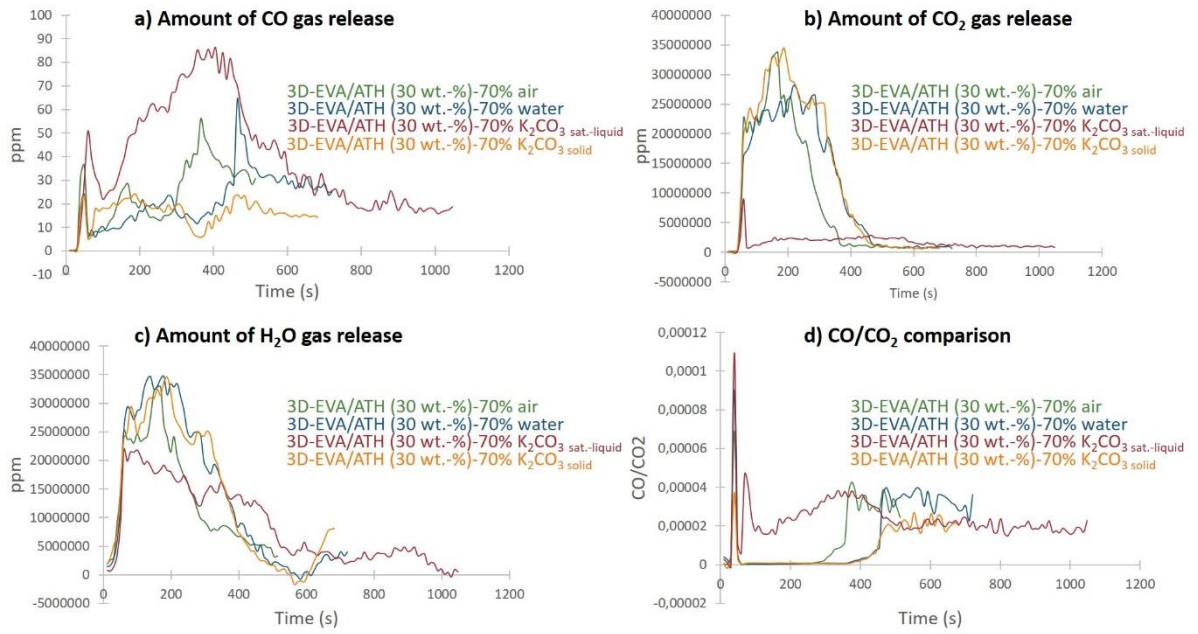

Figure 14. Amount of gas release during MLCC test for each sample studied (a) for CO, b) for CO_2, c) for H_2O)

2.3.2. Condensed phase analysis after fire testing

The mechanism of protection of the materials containing K_2CO_3 were investigated analyzing the condensed phase. Figure 15 shows energy spectra from EDS analysis of all residues obtained after MLCC tests. First of all, C, O and Al were detected for all systems. These

elements were expected and come from alumina (dehydration of ATH) and EVA decomposition [23 - 25]. It is noteworthy no peak between 3.2 and 3.4 keV (K element) was detected for sample with air and water (as expected) while a peak is clearly observed between 3.2 and 3.4 keV. for EVA/ATH (30 wt.-%)-70% $K_2CO_{3\ solid}$ and EVA/ATH (30 wt.-%)-70% $K_2CO_{3\ sat.-liquid}$. These results were confirmed by EDS mapping of K element for each sample studied (Figure 16). In Figure 16 a) and b), the few yellow points observed correspond to the continuous background. In Figure 16 c) and d), K element is clearly identified and observed in these both residues. It evidences that K-based molecules also remain in the condensed phase and they are not all transported into the gas phase.

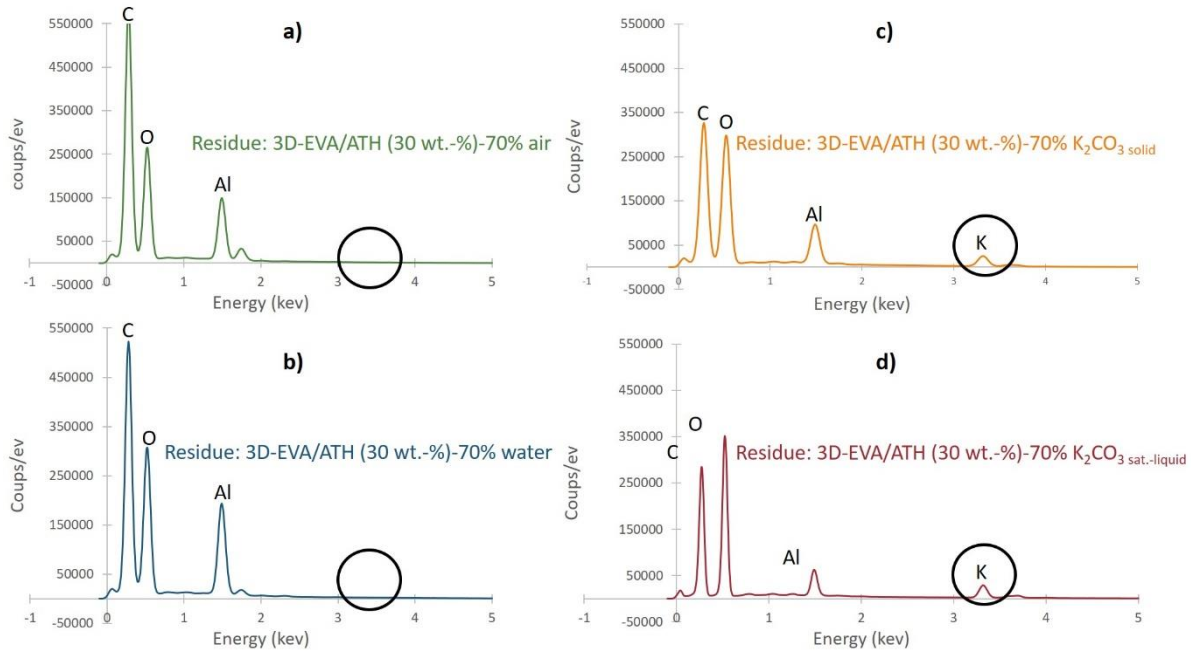

Figure 15. Residue EDS spectra of: a) EVA/ATH (30 wt.-%)-70% air, b) EVA/ATH (30 wt.-%)-70% water, c) EVA/ATH (30 wt.-%)-70% $K_2CO_{3\ solid}$, d) EVA/ATH (30 wt.-%)-70% $K_2CO_{3\ sat.-liquid}$

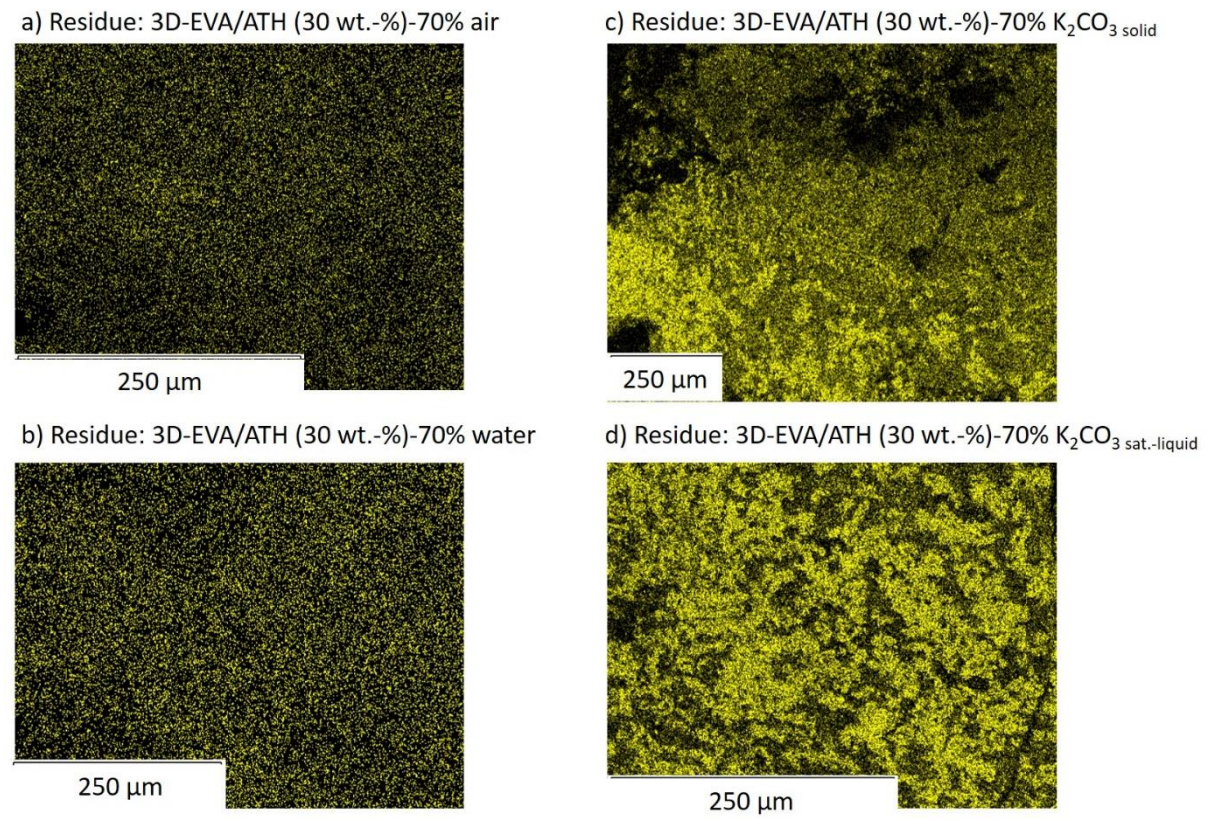

Figure 16. EDS mapping of K after MLCC test in residue of: a) EVA/ATH (30 wt.-%)-70% air, b) EVA/ATH (30 wt.-%)-70% water, c) EVA/ATH (30 wt.-%)-70% $K_2CO_{3\ solid}$, d) EVA/ATH (30 wt.-%)-70% $K_2CO_{3\ sat.-liquid}$

The EVA/ATH (30 wt.-%)-70% $K_2CO_{3\ solid}$ and EVA/ATH (30 wt.-%)-70% $K_2CO_{3\ sat.-liquid}$ residues were analyzed by XRD to investigate the changes of K_2CO_3. Figure 17, 18 and Figure 19 show the X –ray spectra (counts per second as function of $\theta/2\theta$). The two residues exhibit the same spectra (Figure 17) and almost no difference can be distinguished. For the system with $K_2CO_{3\ sat.-liquid}$, broader bands were obtained compared to system with K_2CO_3 solid. It suggests EVA/ATH (30 wt.-%)-70% $K_2CO_{3\ sat.-liquid}$ residue has a higher amorphous phase than EVA/ATH (30 wt.-%)-70% $K_2CO_{3\ solid}$ residue. The amorphous phase detected could be assigned to Al_2O_3 from the ATH dehydration in EVA [23]. In the two residues, three crystalline phases were identified: $KAl(CO_3)(OH)_2$, $KHCO_3$ and $Al(OH)_3$ (Figure 18 and 19). These crystalline structures suggest that: i) K_2CO_3 reacts with ATH and/or alumina to form a potassium aluminum carbonate hydroxide, ii) a part of alumina residue is rehydrated to form $Al(OH)_3$ (according to this reaction: $Al_2O_3 + 3\ H_2O \rightarrow 2\ Al(OH)_3$ [33]), due to water evolution. As a consequence, as the same species are formed in the residues of the two system, it is reasonable to assume that the THR reduction is mainly due to gas phase action of K_2CO_3.

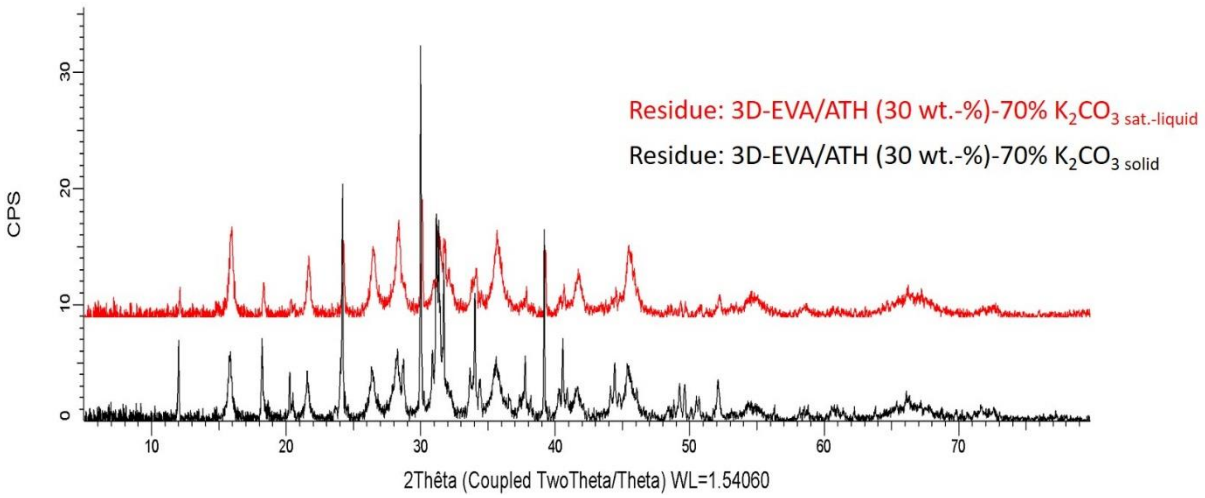

Figure 17. XDR spectra comparison between EVA/ATH (30 wt.-%)-70% $K_2CO_{3\ solid}$ residue and EVA/ATH (30 wt.-%)-70% $K_2CO_{3\ sat.-liquid}$ residue

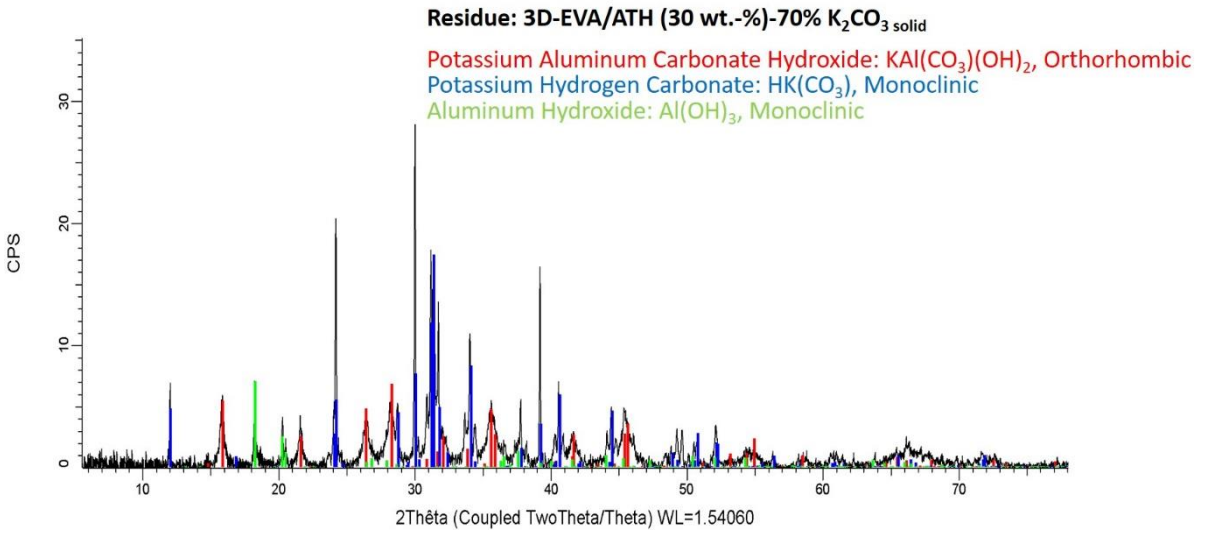

Figure 18. XDR spectrum of EVA/ATH (30 wt.-%)-70% $K_2CO_{3\ solid}$ residue

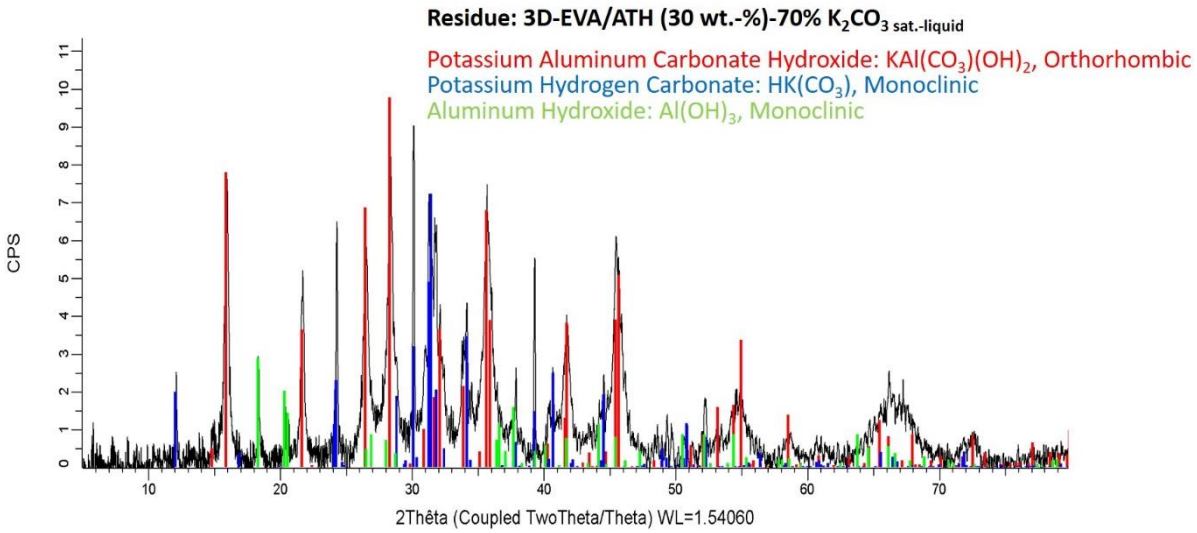

Figure 19. XDR spectrum of EVA/ATH (30 wt.-%)-70% $K_2CO_{3\ sat.-liquid}$ residue

3. Discussion

In this work, the influence of the design of materials in terms of reaction to fire was studied. A lightweight design was tested with voids inside material. In case of EVA/EG (10 wt.-%) a strong decrease of HRR was measured when voids are incorporated inside materials. These differences can be explained by (Figure 20 a)): i) the compacity of entangled network (caused by the graphite expansion) changing, ii) the reduction of the 'fuel' load caused by the design modification, and iii) the lower thermal conductivity of hollow structure comparing to non-hollow structure can delay the heat transfer as long as the voids stand during burning, and hence HRR is decreased. For the material with EVA/ATH (30 wt.-%)-70% air, FR polymer melts and burns, and the voids (created by the new design) are filled. As a consequence, the design is no longer maintained and does not enhance the performance (Figure 20b)). In the case of EVA/ATH (65 wt.-%), EVA also melts and burns but concurrently ATH dehydrates and makes an alumina-type ceramic (Figure 20 c)). In addition to that, fuel load generated by the new design is less. Moreover, as Figure 8 illustrated, the hollow structure is kept during burning. So, it is possible to assume that voids reduce the heat propagation (due to their lower thermal conductivity) and improve the fire retardancy of the materials. Therefore, the combination of water evolution (dilution), ceramization (physical mass transfer barrier) and lower 'fuel' load (caused by the new design) stops the combustion. Thus, with this sandwich material, the change of design allows to increase the fire protection without any formulation modification.

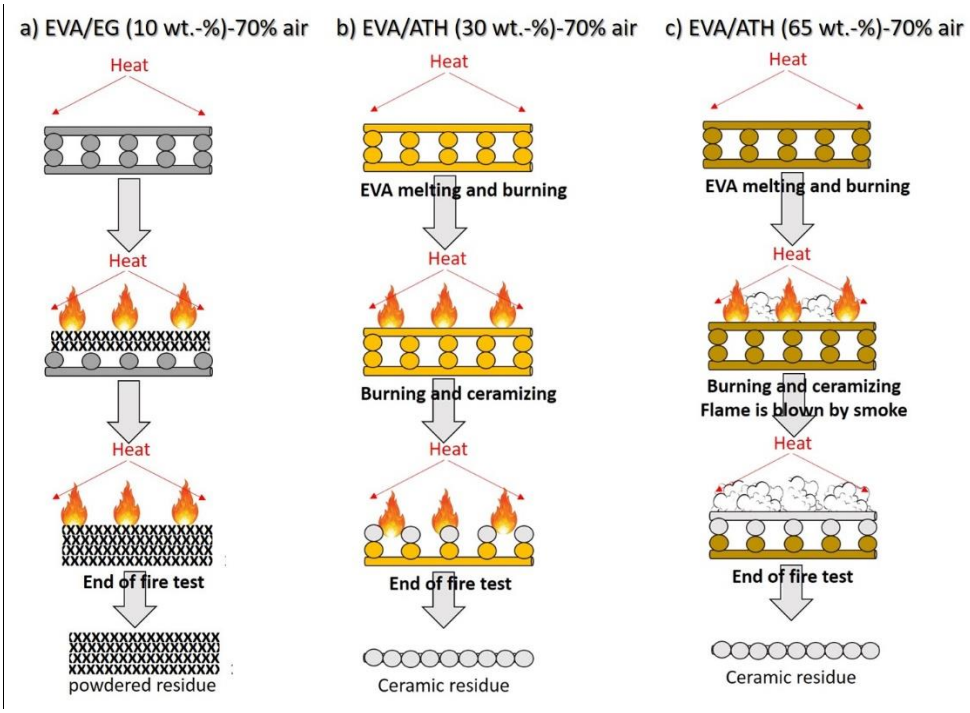

Figure 20. Illustration of fire behavior mechanism for 3D printed plate with 30%polymer (70% voids inside materials) for a) EVA/ATH (30 wt.-%), b) EVA/ATH (65 wt.-%), c) EVA/EG (10 wt.-%)

Based on this very promising design, air was substituted by another phase to create biphasic materials in the case of EVA/ATH (30 wt.-%). As it was previously highlighted, the design of EVA/ATH (30 wt.-%)-70% air has not a significant influence compared to standard design (EVA/ATH (30 wt.-%)-0% air). (Figure 21 a)). In the case of the sample containing only water (Figure 21 b)), EVA melts and burns and water vaporizes. But the amount of water is not enough to play a significant role for enhancing the fire performance (no reduction of HRR). Figure 21 c)) illustrates the case where voids are filled with powdered K_2CO_3. When this sample is heat exposed: the EVA matrix melts and burns, but K_2CO_3 powdered does not decarbonize because the external heat flux is too low to make the decarbonation of K_2CO_3 (891°C). So, no improvement of the fire performance is observed. No potassium-based compound was transported into the gas phase but ATH and/or alumina residue react with powdered K_2CO_3 and form a potassium aluminum carbonate hydroxide which remains in the condensed phase. On the opposite, when K_2CO_3 is solubilized in water, K_2CO_3 is dissociated as: $K_2CO_{3\,(s)} + H_2O \rightarrow KOH + KHCO_3$. When sample ignites, a lot of gases is evolved (visual observation). The solution reaches its boiling temperature and vaporizes leading to the transportation of KOH (or K/H_2O) into the flame (Figure 21 d)) (proven by the color change of flame and soot analysis by EDS). At the same time $KHCO_3$ (transported into the flame by the vapor when the solution evaporated upon heating) decomposes between 100 and 120°C according to the endothermic reaction: $2\ KHCO_3 \rightarrow K_2CO_{3\,(s)} + CO_{2\,(g)} + H_2O_{\,(g)}$. Thus, two

nonflammable gases ($CO_{2\ (g)}$ and $H_2O_{\ (g)}$) were produced and absorbed heat from the fire (dilution of the flame) [34 - 37]. In the same time, the remaining $K_2CO_{3(s)}$ also react with ATH and/or alumina residue and form a potassium aluminum carbonate hydroxide (as EVA/ATH (30 wt.-%)-70% $K_2CO_{3\ solid}$). Overall, the mechanism of action is then: i) KOH (or K/H_2O) is transported into the flame by the vapor (when the solution evaporated upon heating) and react via free radical reactions [35], [36], and ii) the additional release of $CO_{2\ (g)}$ and $H_2O_{\ (g)}$ dilutes the flame and (iii) the combination of these two effects permits the rapid extinguishment of the flame and THR and pHRR are strongly reduced. The main step responsible to the flame extinction is mainly due to the transport of K_2CO_3 (K^+ ionized in water) by the vapor upon heating. It favors then K^+ to interact in the gas phase as it was evidenced in Figure 12 observing the flame color changes.

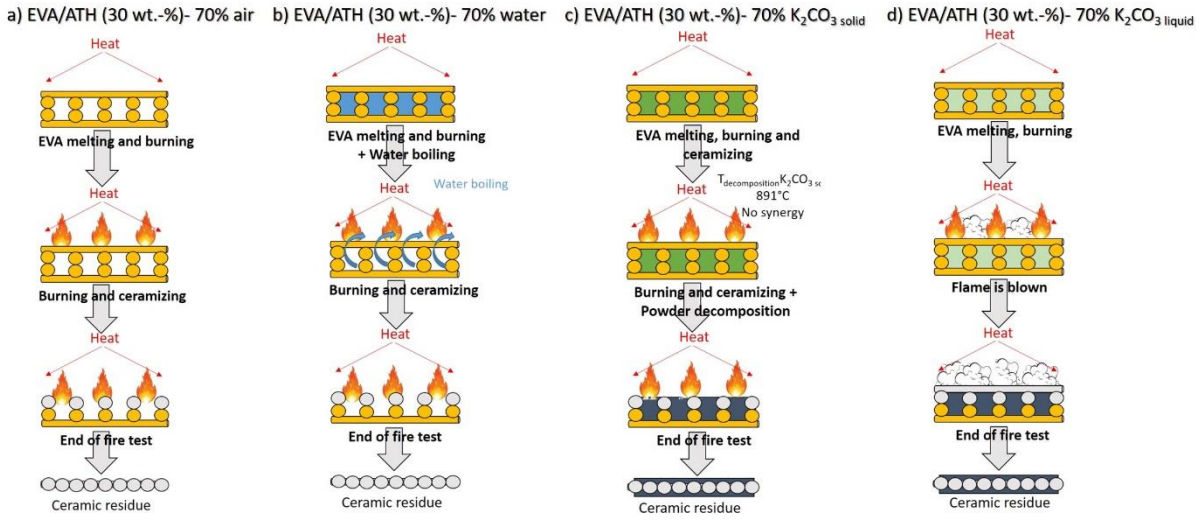

Figure 21. Illustration of fire behavior mechanism of new biphasic multi-materials (a) EVA/ATH (30 wt.-%)-70% air, b) EVA/ATH (30 wt.-%)-70% water, c) EVA/ATH (30 wt.-%)-70% $K_2CO_{3\ powdered}$, d) EVA/ATH (30 wt.-%)-70% $K_2CO_{3\ liquid}$)

Conclusion

A new way of thinking came up in this work. To reach better reaction to fire, the influence of design was tested instead of changing the material formulation as it is usually done. A new design was elaborated with voids inside materials to reduce both the weight of the flame retardant materials (EVA/EG (10 wt.-%), EVA/ATH (30 wt.-%) and EVA/ATH (65 wt.-%)) and to create bi-phasic systems. Two different plates were printed (such as sandwich materials) and composed of two shells completely fill with 100% polymer, and core with a

certain amount of polymer inside (50% or 30%). These designs were evaluated according to the cone calorimeter scenario, and reveal better fire protection performances than standard design. New biphasic materials were then elaborated with EVA/ATH (30 wt.-%)-70% air as basic material. The voids were filled with water or potassium carbonate in solid or liquid phase. The system with potassium carbonate in liquid phase reveals the fast flame extinguishment (due to H_2O and CO_2 emission and the release of K and KOH into the flame) and hence, this material exhibits extremely low HRR and THR during the heat exposure. Thank to this work, the advantage of additive manufacturing is highlighted, and proved that it is possible to elaborate an efficient fire reacted material and improve flame retardancy by design modification rather than just changing materials chemistry.

Funding

This work has received funding from the European Research Council (ERC) under the European Union's H2020- the framework programme for Research and Innovation (2014-2020) ERC Grant Advances Agreement N°670747-ERC 2014 AdG/FireBar-Concept for FireBar Concept project.

Acknowledgements

We would thank the SEM facility in Lille (France) which is supported by the conseil Régional du Nord-Pas de Calais, and the European Regional Developmen Fund (ERDF). We would also like to thank Manon Saget for her help with SEM observations.

Author contributions

LG carried out all of this work. She performed the scientific discussion and conclusion, and wrote the paper. SB, MJ, and FS supervised the work and contributed to the paper written by LG.

References

[1] J. Alongi, Z. Han, and S. Bourbigot, "Progress in Polymer Science Intumescence: Tradition versus novelty: A comprehensive review," *Prog. Polym. Sci.*, vol. 51, pp. 28–73, 2015.

[2] K. M. Holder, R. J. Smith, and J. C. Grunlan, “Review A review of flame retardant nanocoatings prepared using layer-by-layer assembly of polyelectrolytes,” *J. Mater. Sci.*, 2017.

[3] S. Duquesne, *Multifunctional Barriers for Flexible Structure*, Springer. 2007.

[4] P.R. Hornsby and R.N. Rothon, Fire Retardant Fillers for Polymers, in: M. Le Bras, S. Bourbigot, S. Duquesne, C. Jama, C. Wilkie (Eds.), Fire Retard. Polym., Royal Society of Chemistry, Cambridge, 2005: pp. 19-41.

[5] M. Gomes et al. Co-injection molding of immiscible polymers: Skin-core structure and adhesion studies, Polym. Eng. Sci. 51 (2011) 2398-2407.

[6] J. Liu et al. A preliminary study on the thermal degradation behavior and flame retardancy of high impact polystyrene/magnesium hydroxide/microencapsulated red phosphorus composite with a gradient structure, Polym. Degrad. Stab. 105 (2014) 21-30.

[7] Z. Yu et al., Thermo-oxidative degradation behavior and fire performance of high impact polystyrene/magnesium hydroxide/microencapsulated red phosphorus composite with an alternating layered structure, Polym. Degrad. Stab. 115 (2015) 54-62.

[8] Lorraine F. Francis, “Materials processing, a unified approach to processing of Metals, Ceramics and Polymers”, Chapter 3 – Melt Processes, Academic Press, 2016, pages 105-249.

[9] T. D. Ngo, A. Kashani, G. Imbalzano, K. T. Q. Nguyen, and D. Hui, “Additive manufacturing (3D printing): A review of materials, methods, applications and challenges,” *Compos. Part B*, vol. 143, no. December 2017, pp. 172–196, 2018.

[10] B. Zhang, S. Liu, and Y. C. Shin, “In-Process monitoring of porosity during laser additive manufacturing process,” *Addit. Manuf.*, vol. 28, no. May, pp. 497–505, 2019.

[11] A. Yaghi, S. Ayvar-soberanis, S. Moturu, R. Bilkhu, and S. Afazov, “Design against distortion for additive manufacturing,” *Addit. Manuf.*, vol. 27, no. February, pp. 224–235, 2019.

[12] Y. Guo *et al.*, “Engineering flame retardant biodegradable polymer nanocomposites and their application in 3D printing,” *Polym. Degrad. Stab.*, vol. 137, pp. 205–215, 2017.

[13] L. Geoffroy and S. Bourbigot, “Additive manufacturing of fire - retardant ethylene - vinyl acetate,” *Polym. Adv. Technol.*, vol. 30, no. 7, pp. 1878–1890, 2019. https://doi.org/10.1002/pat.4620

[14] A. Regazzi et al. Controlling the distribution of fire retardants in PLA by fused filament fabrication in order to improve fire behaviour, Polym. Degrad. Stab. 163 (2019) 143-150

[15] 1. Lao, S. C., Koo, J. H., Moon, T. J., Londa, M., Ibeh, C. C., Wissler, G. E., & Pilato, L. A. (2011). Flame-retardant polyamide 11 nanocomposites: further thermal and flammability studies. Journal of Fire Sciences, 29(6), 479-498. https://doi.org/10.1177/0734904111404658

[16] Richardson, M. J., Wu, H., Wilcox, T. J., Broaddus, M., Lin, P. C., Krifa, M., & Koo, J. H. (2017). Flame Retardant Nylon 6 Nanocomposites for Fused Deposition Modeling (FDM) Applications. SAMPE 2017.

[17] Wu, H., Sulkis, M., Driver, J., Saade-Castillo, A., Thompson, A., & Koo, J. H. (2018). Multi-functional ULTEM™ 1010 composite filaments for additive manufacturing using Fused Filament Fabrication (FFF). Additive Manufacturing, 24, 298-306.

[18] Wu, H., Kafi, A.A., Kim, H., Shah, R.M., Bateman, S.A., & Koo, J. (2019). Additive Manufacturing of Flame-retardant Polyamide 6 Nanocomposites Via Fused Filament Fabrication (FFF). SAMPE 2019. DOI: 10.33599/nasampe/s.19.1573

[19] Clariant company website. « PA6 FR using Exolit », [on line]: https://www.clariant.com/en/Solutions/Products/2018/01/22/04/34/PA6_FR_Exolit_3DPrinter Filament, [consulted on the 06/28th/2019]

[20] Arkema company website. "Thermoplastic pellets for filaments extrusion", [on line]: https://www.arkema.com/en/markets-and-solutions/solutions/3d-printing/extrusion/, [consulted on the 06/28th/2019]

[21] Z. J. Lobos, "United States Patent Office: Dry chemical fire extinguisher composition," 1965.

[22] R.Tay, Business insider France, "Samsung designed a vase that can be throw at fires to extinguish them", 3 April 2019, [on line] http://www.businessinsider.fr/us/samsung-designed-a-vase-that-can-be-thrown-at-fires-to-extinguish-them-2019-4, [consulted on the 07/16th/2019]

[23] B. Girardin, G. Fontaine, S. Duquesne, M. Försth, and S. Bourbigot, "Characterization of Thermo-Physical Properties of EVA / ATH : Application to Gasification Experiments and Pyrolysis Modeling," pp. 7837–7863, 2015.

[24] F. Taschner, C. Hoffendahl, S. Duquesne, M. Mezger, and S. Bourbigot, “Decomposition mechanism of fi re retarded ethylene vinyl acetate elastomer (EVA) containing aluminum trihydroxide and melamine,” vol. 113, pp. 168–179, 2015.

[25] L. Gay, S. Bourbigot, and F. Ngohang, “Smoke composition using MLC / FTIR / ELPI: Application to flame retarded ethylene vinyl acetate,” vol. 115, pp. 89–109, 2015.

[26] S. Bourbigot, J. Sarazin, F. Samyn, and M. Jimenez, “Intumescent ethylene-vinyl acetate copolymer: Reaction to fi re and mechanistic aspects,” *Polym. Degrad. Stab.*, vol. 161, pp. 235–244, 2019.

[27] Norme ISO 13927. Plastic-simple heat release test using a conical radiant heater and a thermopile detector, 2014

[28] Norme ISO 5660-1. Reaction-to-fire-tests-heat release, smoke production and mass loss rate, 2002

[29] G. Okyay, S. Bellayer, F. Samyn, M. Jimenez, and S. Bourbigot, “Characterization of in- flame soot from balsa composite combustion during mass loss cone calorimeter tests,” *Polym. Degrad. Stab.*, vol. 154, pp. 304–311, 2018.

[30] S. Kang, J. Y. Choi, and S. Choi, “Mechanism of Heat Transfer through Porous Media of Inorganic Intumescent Coating in Cone Calorimeter Testing,” *Polymers (Basel).*, vol. 11, no. 2, 2019.

[31] A-M. Helmenstine, “How flame test colors are produced”, Science, tech, Math, 2019

[32] W. Periodicals, “Is Scanning Electron Microscopy / Energy Dispersive X-ray Spectrometry (SEM / EDS) Quantitative ?,” vol. 35, pp. 141–168, 2013.

[33] J. A. Aad, “Dégradation chimique et mécanique de l ’ alumine en phase aqueuse : mécanisme et inhibition en conditions ambiantes et hydrothermales To cite this version : HAL Id : tel-01913067 Université Pierre et Marie Curie Dégradation chimique et mécanique de l ’ al,” 2018.

[34] Z. Tianwei, L. Hao, H. Zhiyue, D. Zhiming, and W. Yong, “Active substances study in fire extinguishing by water mist with potassium salt additives based on thermoanalysis and thermodynamics,” *Appl. Therm. Eng.*, vol. 122, pp. 429–438, 2017.

[35] K. van W. V. I. Babushok, G. T. Linteris, P. Hoorelbeke, D. Roosendans, “Flame inhibition by Potassium-Containing Compounds,” *Combust. Sci. Technol.*, vol. 2202, no. July, 2017.

[36] J. D. Birchah, “On the Mechanism of Flame Inhibition by Alkali Metal Salts,” 1970.

[37] J. W. Hastie, “Molecular Basis of Flame Inhibition,” vol. 77, no. 0, pp. 733–754, 1973.